

Chapter 2

Quantum Chemistry of Solids

Abstract Energy band theory is introduced as an extension of the molecular orbital theory, and applied to organic conductors. From this, we can discuss the Fermi surface of organic conductors.

Keywords Energy band · Tight-binding approximation · Bloch condition · Bandwidth · Hückel rule · Periodical boundary condition · Density of states · Free-electron model · Fermi-Dirac distribution · Bose-Einstein distribution · Boltzmann distribution · Transfer integral · Hole · Fermi surface · Brillouine zone · Peierls transition

2.1 Tight-Binding Approximation

In the last chapter, we have investigated molecular orbitals of π -conjugated rings with the carbon number from $N = 3$ (cyclopropenyl cation) to $N = 6$ (benzene). In this chapter, we shall investigate energy levels of π -conjugated rings for general N [1, 2]. The solution affords energy levels of large π -systems in which the secular equation is not easily solved. The solution also provides a general proof of the Hückel $4n + 2$ rule. Large N leads to a large π -conjugated ring (Fig. 2.1a). The linear chain corresponds to polyacetylene (Fig. 2.1b), while linear polyacetylene has terminal states (Fig. 2.1c). The ordinary carbon atom is bonded to one hydrogen and two carbon atoms, whereas the terminal carbon is connected to two hydrogen and one carbon atoms. Then, the terminal has a different electronic state. In order to avoid such a terminal state, a ring is considered (Fig. 2.1a). When N is as large as the Avogadro number, this leads to energy bands in a bulk solid. Hereafter, a is the distance between the adjacent carbon atoms.

Since this is a natural extension of the Hückel approximation, we consider each carbon atom to have one π orbital. The LCAO-MO is constructed from N orbitals.

$$\psi = \sum_n^N c_n \chi_n \quad (2.1)$$

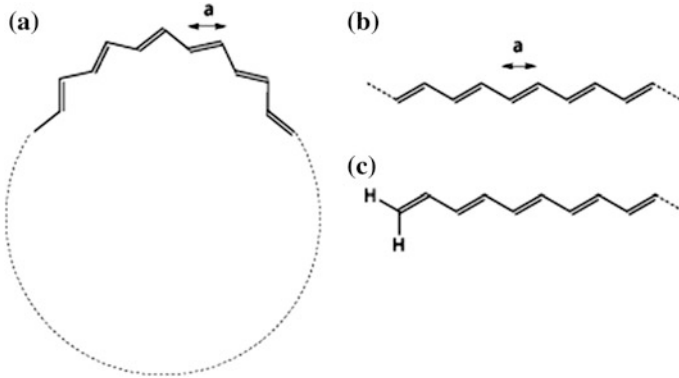


Fig. 2.1 (a) A π -conjugated ring with the carbon number N , (b) a linear π -system, polyacetylene, and (c) edge states of the polyacetylene

The secular equation is obtained in the form of an $N \times N$ determinant.

$$\begin{vmatrix} \alpha - E & \beta & 0 & \dots \\ \beta & \alpha - E & \beta & \dots \\ 0 & \beta & \alpha - E & \dots \\ \vdots & \vdots & \vdots & \vdots \end{vmatrix} = 0 \quad (2.2)$$

It is possible to solve this equation for general N , but we will adopt another easier way.

The system has a periodicity of a . Then, after the translation of $r \rightarrow r + a$, the resulting function $\psi(r + a)$ is again the eigenfunction. The Hamiltonian also has the periodicity, so the translation $r \rightarrow r + a$ does not change the energy. Accordingly, $\psi(r)$ and $\psi(r + a)$ are eigenfunctions with the same energy. If there is no degeneracy,¹ these two functions are related to each other like $\psi(r + a) = c(a)\psi(r)$ using a constant $c(a)$. One more translation results in $\psi(r + 2a) = c(2a)\psi(r)$, which leads to $\psi(r + 2a) = c(a)\psi(r + a) = c(a)c(a)\psi(r)$. Thus, we obtain $c(2a) = c(a)c(a)$. When $c(a) = e^{ika}$ is assumed, this $c(a)$ satisfies the above relation. As a consequence, we obtain $\psi(r + a) = e^{ika}\psi(r)$; this condition is known as the **Bloch condition**.

This is a general relation derived from the periodicity. The LCAO (Eq. 2.1) satisfying this condition is represented as

$$\begin{aligned} \psi &= c_0 [\chi_0 + e^{ika}\chi_1 + e^{i2ka}\chi_2 + e^{i3ka}\chi_3 + e^{i4ka}\chi_4 + \dots] \\ &= c_0 \sum_n e^{in ka} \chi_n. \end{aligned} \quad (2.3)$$

¹This assumption is not strictly correct because the states at k and $-k$ are generally degenerate. Nonetheless, this assumption gives the correct conclusion if the unnecessary hybridization of the degenerate states is appropriately avoided.

This form of wave function will be called a **crystal orbital** in contrast to the molecular orbital. Here, e^{ika} is a complex whose absolute value is one, and the phase is nonzero. After the translation of a , the amplitude does not change, but the phase changes. Here, k is introduced as a coefficient which determines the phase shift ka . Since ka is dimensionless, k has a unit of inverse length. This quantity is identical to the wave number introduced in the last chapter.

Usually, we solve the secular equation and then obtain the wave function. In contrast, here the wave function has been mostly determined from the periodicity. Once the wave function ψ is known, the energy is obtained by multiplying ψ^* to $H\psi = E\psi$ from the left and integrating it in the whole space.

$$E = \frac{\int \psi^* H \psi d\tau}{\int \psi^* \psi d\tau} \quad (2.4)$$

When Eq. 2.3 is substituted in Eq. 2.4, we obtain

$$E = \frac{\int (\sum_m e^{-imka} \chi_m^*) H (\sum_n e^{inka} \chi_n) d\tau}{\int (\sum_m e^{-imka} \chi_m^*) (\sum_n e^{inka} \chi_n) d\tau} = \frac{\sum_n \sum_m e^{i(n-m)ka} \int \chi_m^* H \chi_n d\tau}{\sum_n \sum_m e^{i(n-m)ka} \int \chi_m^* \chi_n d\tau}. \quad (2.5)$$

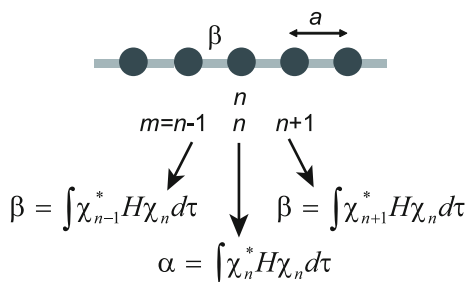
We focus on a given n (Fig. 2.2). According to the usual definition of the Hückel approximation, $\int \chi_m^* H \chi_n d\tau$ is α for $m = n$, and β for $m = n \pm 1$, namely for the adjacent atoms. This integral is zero for all other combinations, because they are not directly bonded. Since the factors e^{ika} and e^{-ika} appear for $m = n \pm 1$, we obtain

$$E = \frac{N(e^{ika}\beta + \alpha + e^{-ika}\beta)}{N}. \quad (2.6)$$

The denominator is N because the overlap integral is one for $m = n$ and zero for all others. Namely, for a given n , a rotation for m affords one. When added for n , this gives N . For a given n , the numerator affords βe^{ika} , α , and βe^{-ika} corresponding to $m = n - 1$, n , and $n + 1$, respectively. When added for a rotation of n , the same terms appear N times. Thus, N cancels with the denominator. The resulting energy is

$$E = \alpha + 2\beta \cos ka \quad (2.7)$$

Fig. 2.2 Integrals appearing in the tight-binding approximation



where $\cos ka = \frac{e^{ika} + e^{-ika}}{2}$ is used. Equation 2.7 is an important relation which represents the energy of the **tight-binding approximation**. This name comes from the starting atomic orbitals, which are tightly bound to the atoms. In solid-state physics, this name is used in contrast to the free-electron approximation, but it is practically equivalent to the LCAO approximation. Therefore, the tight-binding approximation is the solid state version of the molecular orbital theory. The original Hamiltonian \mathbf{H} includes the potential energy of N atoms. However, following the standard Hückel approximation, the energy is represented by a simple function of α and β . We shall investigate the meaning of this equation as follows.

Equation 2.7 affords a cosine curve as shown in Fig. 2.3a. The cosine curve is upside down because β is negative. The energy is $E = \alpha + 2\beta$ at $k = 0$, where the energy takes minimum. The maximum energy is $E = \alpha - 2\beta$, which appears at $ka = \pm\pi$, namely at $k = \pm\pi/a$. Although this is a periodical function, it is sufficient to consider the region of $-\pi/a < k < \pi/a$. In Fig. 2.3, only this region is plotted.

Since the atoms form a ring (Fig. 2.1a), the atom at $N + 1$ is identical to the first atom, and the N -th atom corresponds to the zero-th atom (Fig. 2.3b). The condition to equate the phases of the N -th atom and the zero-th atom is satisfied when $e^{iNka} = 1$. This is fulfilled when $Nka = 2\pi n$, where n is an integer. This leads to $k = 2\pi n/Na$. The restriction on k is called the **periodical boundary condition**. When N is large, $2\pi/Na$ is very small, though k is restricted to the integer times of this quantity. Figure 2.3a shows the discrete energy levels aligned with this k interval. In a solid, N is as large as the Avogadro number, and k is practically continuous. Since the energy levels are almost continuous, this is called an **energy band**. Since the energy band exists in the range of $\alpha + 2\beta < E < \alpha - 2\beta$, the **bandwidth** is $4|\beta|$.

Even though the energy band is practically continuous, each energy level has the wave function. For example, at $k = 0$, e^{inka} is always one, so the corresponding wave function (Eq. 2.3) is

$$\varphi = \chi_0 + \chi_1 + \chi_2 + \chi_3 + \cdots \quad (2.8)$$

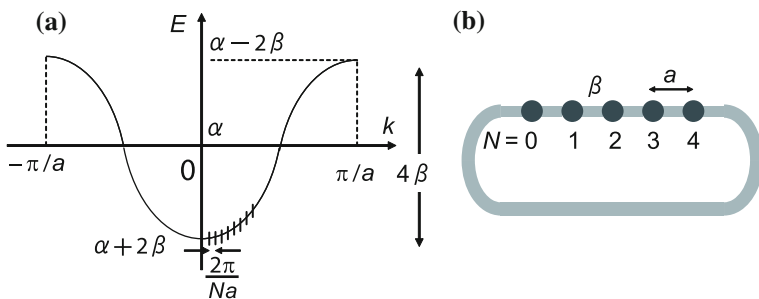


Fig. 2.3 (a) $E(k)$ in the one-dimensional tight-binding approximation, and (b) the periodical boundary condition

This is a bonding orbital spreading over the whole solid (Fig. 2.4). For $k = \pm\pi/a$, $nka = n\pi$ leads to $e^{inka} = 1, -1, 1, -1$, so the wave function is

$$\varphi = \chi_0 - \chi_1 + \chi_2 - \chi_3 + \dots \tag{2.9}$$

This is an antibonding orbital where a node is located on every carbon-carbon bond (Fig. 2.4). This is the reason that this state has the highest energy. In the energy level next to $k = 0$, the phase of the successive carbon increases by $e^{i2\pi/N}$, and the whole rotation leads to the 2π phase shift. The corresponding wave function has two nodes during the rotation. Due to the small number of nodes, we have to gradually increase the phase, and the coefficient of a crystal orbital has to be a complex number. In general, a coefficient of a molecular orbital is real, whereas a coefficient of an orbital in a solid is complex. In the succeeding energy levels, the phase shift increases as $4\pi, 6\pi \dots$ during the rotation, and the node number increases as $4, 6 \dots$. The final level at $k = \pi/a$ has N nodes, and a node is located on every carbon-carbon bond.

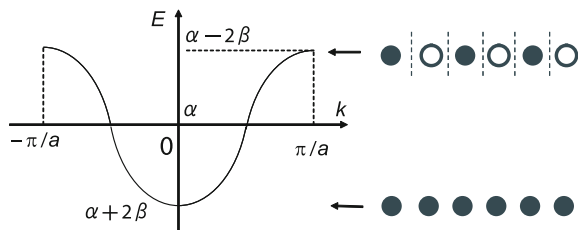
We shall investigate the number of energy levels in the energy band. Since the interval of the energy levels is $2\pi/Na$, the number of the energy levels existing between $k = -\pi/a$ and $k = \pi/a$ is

$$\frac{2 \times \frac{\pi}{a}}{\frac{2\pi}{Na}} = N. \tag{2.10}$$

The carbon number is N , and the number of the atomic orbitals is N . Therefore, it is quite reasonable that the number of the energy levels is N in analogy with the number of solutions obtained from a secular equation (Eq. 2.2). This justifies that we consider only the region of $-\pi/a < k < \pi/a$. This region is called the **first Brillouin zone**.

In polyacetylene, each carbon atom has one π electron. Thus, the total number of the π electrons is N . The occupation of the energy band is shown in Fig. 2.5a. When we place electrons from the lowest levels, the energy levels are occupied up to a certain energy, above which the levels are unoccupied. The border energy is called

Fig. 2.4 Orbitals in a one-dimensional tight-binding band



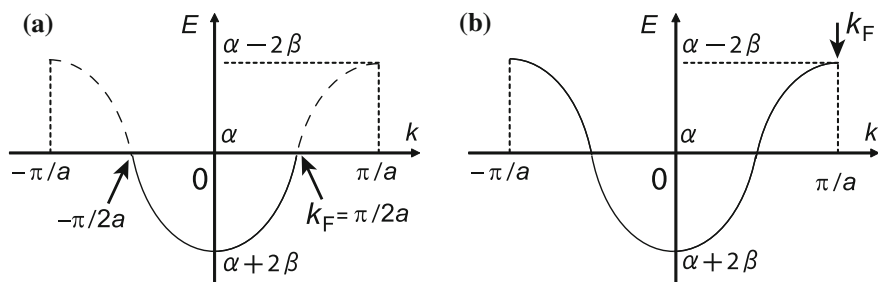


Fig. 2.5 (a) A half-filled one-dimensional tight-binding band, and (b) an entirely filled one-dimensional tight-binding band

the **Fermi energy** E_F , and the corresponding k is the **Fermi wave number** k_F . Since the N electrons enter the $-k_F < k < k_F$ range, we obtain

$$2 \frac{2k_F}{\frac{2\pi}{Na}} = N \quad (2.11)$$

where two before the fraction comes from the upspin and downspin electrons entering an energy level. Solving this relation, we obtain

$$k_F = \frac{\pi}{2a} \quad (2.12)$$

so, k_F is half of π/a . Therefore, the Fermi energy appears at the band center at $E_F = \alpha$. This situation is called **half-filled**. Since the energy band is continuous around E_F , a half-filled energy band is a metallic band. However, actual polyacetylene is an insulator unless doped. This discrepancy will be resolved in the later part of this chapter.

When the total electron number is $2N$, we obtain similarly

$$2 \frac{2k_F}{\frac{2\pi}{Na}} = 2N. \quad (2.13)$$

This is reduced to $k_F = \pi/a$. Here, the energy band is entirely occupied (Fig. 2.5b). In this situation, each energy level has two electrons. This is the entirely occupied state. Most organic compounds are closed shell molecules, and the HOMO is occupied like this. Ordinary molecular crystals have such a state and they are insulators.

In the above discussion, the tight-binding approximation is applied to an energy band in a solid. However, Eq. 2.7 is also valid for small N . For example, $N = 6$ corresponds to benzene, where k is restricted to $k = \frac{2\pi n}{Na} = \frac{2\pi n}{6a}$. Then, the phase in

the cosine function rotates by an interval of $ka = \pi/3$. Substituting this in Eq. 2.7, we obtain

$$E = \alpha + 2\beta \cos \frac{2\pi}{6} n. \quad (2.14)$$

As shown in Fig. 2.6, the energy for $n = 0, \pm 1, \pm 2, \text{ and } 3$ leads to

$$E = \alpha + 2\beta, \alpha + \beta, \alpha + \beta, \alpha - \beta, \alpha - \beta, \alpha - 2\beta. \quad (2.15)$$

These results are the same as Example 1.8.

In Fig. 2.7, energy levels of π -conjugated rings are depicted for $N = 4, 6, \text{ and } 8$. Since a cosine function is a real part of e^{ika} , it is convenient to suppose a complex plane of $x + iy$, whose real axis x is taken downwards (Fig. 2.7b). Starting from the x direction corresponding to $n = 0$, the circle is equally divided by N , and the height affords the energy levels. For $N = 4$, the energy levels appear at the successive $\pi/2$ positions, so two energy levels appear at $E = \alpha$. These levels are half-filled, but due

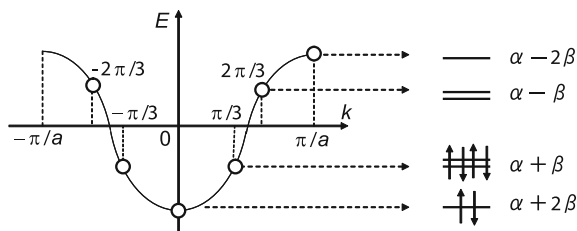


Fig. 2.6 Molecular orbital levels of benzene obtained from the tight-binding approximation

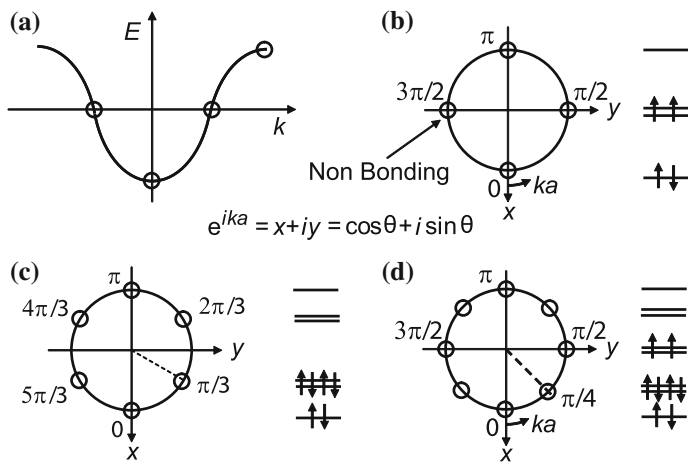


Fig. 2.7 Energy levels of (a) cyclobutadiene ($N = 4$), (c) benzene ($N = 6$), and (d) cyclooctatetraene ($N = 8$) obtained from the tight-binding approximation

to the nonbonding character, the delocalization energy becomes zero. For $N = 6$, an energy gap appears at $E = \alpha$ (Fig. 2.7c). Then, all electrons enter the bonding levels below $E = \alpha$, to give rise to the delocalization energy. For $N = 8$, the energy levels appear at the successive $\pi/4$ positions (Fig. 2.7d), and two energy levels appear at $E = \alpha$. Therefore, the delocalization energy is zero. Zero delocalization energy occurs at $N = 4n$, while the delocalization energy appears at $N = 4n + 2$ in the aromatic rings. This is the most general proof of the Hückel rule.

Example 2.1 Calculate the energy levels of cyclopentadienyl anion using the tight-binding approximation. Calculate the bonding energy and compare it with those of the radical and the cation. The same molecule has been previously discussed in Example 1.15.



For $N = 5$, k is limited to $k = \frac{2\pi n}{5a}$, so the energy is $E = \alpha + 2\beta \cos \frac{2\pi}{5} n$. The values for $n = 0, \pm 1$, and ± 2 are shown in Fig. 2.8.

In a radical, every carbon atom gives up one π electron, and the total number of the π electrons is five. An anion has one additional electron, and the π electron number is six, whereas a cation has four electrons. These four to six electrons occupy the π levels as shown in Fig. 2.8. The bonding energy is estimated by summing the energy of the occupied levels.

$$\begin{array}{lll}
 \text{Anion} & 6\pi & 2(\alpha + 2\beta) + 4(\alpha + 0.618\beta) - 6\alpha = 6.472\beta \\
 \text{Radical} & 5\pi & 2(\alpha + 2\beta) + 3(\alpha + 0.618\beta) - 5\alpha = 5.854\beta \\
 \text{Cation} & 4\pi & 2(\alpha + 2\beta) + 2(\alpha + 0.618\beta) - 4\alpha = 5.236\beta
 \end{array} \quad (2.16)$$

Since bonding energy of three double bonds is 6β , the anion has larger bonding energy than this, showing large delocalization energy.

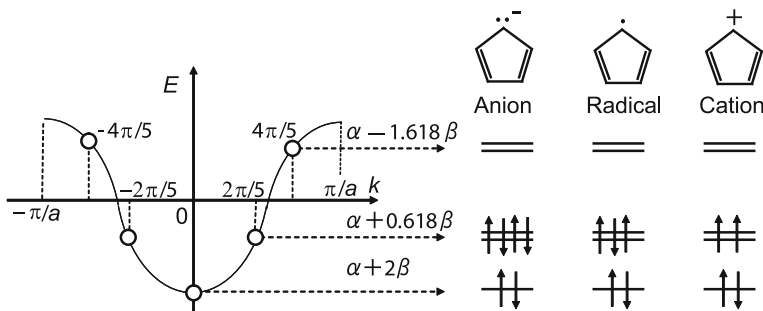


Fig. 2.8 Energy levels in the cyclopentadienyl anion, radical, and cation

Fig. 2.9 Azulene



A cyclopentadienyl anion shows aromaticity owing to the six π electrons. Actually, this is an extraordinarily stable organic anion. It forms an ionic compound with Fe^{2+} with the composition of $\text{Fe}(\text{C}_5\text{H}_5)_2$. This entirely air-stable orange solid is known as ferrocene. Ferrocene is used as a standard material of electrochemistry (Sect. 7.2). Ferrocene dissolves in organic solvents, and Fe^{2+} is electrochemically oxidized to Fe^{3+} .

The original Hückel rule tells us that π -conjugated systems with the carbon number $4n + 2$ show aromaticity. The above example shows that π -conjugated systems with the π electron number $4n + 2$ are stable in a similar way. As another example, in azulene (Fig. 2.9), the five-membered ring tends to have six π electrons like a cyclopentadienyl anion, and the seven-membered ring is stabilized in the cationic 6π form. Azulene is a hydrocarbon with the formula of C_{10}H_8 , which is an isomer of naphthalene containing only carbon and hydrogen. Nonetheless, azulene is a very polar molecule. A five-membered ring makes a stable anion with 6π electrons, and a seven-membered ring makes a stable cation with 6π electrons. Accordingly, we can make stable organic anions and cations. Design of organic electron donors and acceptors based on this principle is investigated in Chap. 7.

2.2 Free-Electron Model

The one-dimensional free-electron model was discussed in Chap. 1. Here, we investigate the three-dimensional free-electron model [3–7]. Total energy of a three-dimensional electron is

$$E = \frac{p_x^2 + p_y^2 + p_z^2}{2m} + V \quad (2.17)$$

and the Schrödinger equation is

$$\left[-\frac{\hbar^2}{2m} \left(\frac{\partial^2}{\partial x^2} + \frac{\partial^2}{\partial y^2} + \frac{\partial^2}{\partial z^2} \right) + V \right] \psi = E\psi. \quad (2.18)$$

Electrons in solids are bound to the nucleus by the Coulomb attraction. In a metal electron, however, the attraction is largely shielded by other core electrons. As a result, a metal electron is approximated by a free electron in a constant potential

V . V is a negative constant, but we take the V value as energy zero, and use $V = 0$ in Eq. 2.18. The eigenfunction of the free electron is

$$\psi(x, y, z) = e^{i(k_x x + k_y y + k_z z)}. \quad (2.19)$$

The eigenvalue is

$$E = \frac{\hbar^2}{2m} (k_x^2 + k_y^2 + k_z^2). \quad (2.20)$$

As shown in Fig. 2.10, the energy is represented by a parabola along the k_x , k_y , and k_z axes. When we include E , we could not plot the function in the four-dimensional space, but we imagine that the respective point (k_x, k_y, k_z) in the three-dimensional k -space has the characteristic energy proportional to the distance from the origin (Eq. 2.20). This is a discussion within fundamental quantum mechanics, but consideration of N electrons introduces solid-state physics.

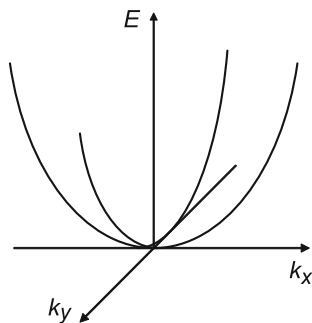
Here, we suppose the electron is not in an infinite space, but enclosed in a box with the length L . The boundary at $x = L$ is not a wall but connected to $x = 0$ as shown in Fig. 2.11a, b. This is the periodical boundary condition, which is necessary to avoid the surface state. This condition requires $\psi(x + L, y, z) = \psi(x, y, z)$, which is satisfied when $e^{ik_x L} = 1$. This leads to $k_x = \frac{2\pi}{L}n$, where n is an integer. This is equivalent to the previous periodical boundary condition by noting $L = Na$. We apply similar conditions to k_y and k_z , and obtain

$$k_x = \frac{2\pi}{L}n_x, k_y = \frac{2\pi}{L}n_y, \text{ and } k_z = \frac{2\pi}{L}n_z \quad (2.21)$$

using three integers, n_x , n_y , and n_z . We assumed the same L for three directions, so we suppose a cube with the edge L .

The periodical boundary condition in three directions is defined like this. However, it is difficult to imagine a cube whose edges are circularly connected in three directions. In a two-dimensional space, we can rotate a donut surface in two different directions (Fig. 2.11c). Then, we imagine a similar surface in the

Fig. 2.10 Free electron energy



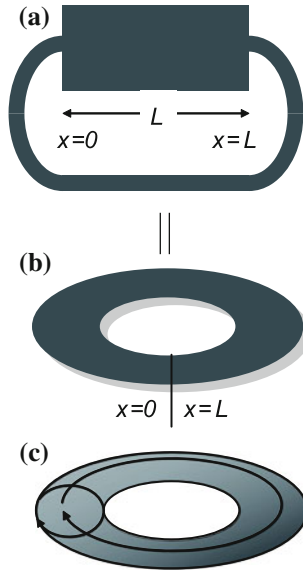


Fig. 2.11 Periodical boundary condition

three-dimensional space. In general, we implicitly believe we live in a Euclidean space spreading to infinity. However, we can trace a spherical surface along a great circle in any directions to come back to the starting position. A spherical surface is two dimensional, but the surface of a four-dimensional sphere is three-dimensional. On this surface, we go to the right and return from the left, going to the front and returning from the back, and going up and returning from underneath. Einstein imagined such a space in his general theory of relativity.

Returning to the original subject, Eq. 2.21 implies that the k -space is restricted to discrete points with the interval of $2\pi/L$ (Fig. 2.12a). In the three-dimensional k -space, the energy level exists only on the lattice points (k_x, k_y, k_z) with the interval

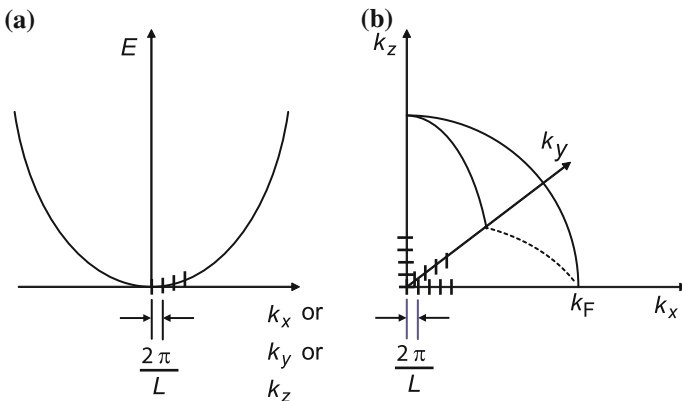


Fig. 2.12 Lattice points and the Fermi surface in the three-dimensional k -space

of $2\pi/L$ (Fig. 2.12b). The energy of the respective point is given by Eq. 2.20, which is proportional to the distance from the origin. When N electrons are incorporated, starting from the origin, each level is occupied by two electrons according to the Pauli exclusion principle. The resulting occupied states have a spherical shape. The boundary between the occupied and unoccupied states is called the **Fermi surface**. The Fermi surface of the three-dimensional free-electron model is a sphere. When the radius of this sphere is k_F , the volume is $\frac{4\pi}{3}k_F^3$. Since each $(\frac{2\pi}{L})^3$ volume contains an energy level, the volume of the Fermi surface is related to the electron number N .

$$2 \frac{\frac{4\pi}{3} k_F^3}{(\frac{2\pi}{L})^3} = N \quad (2.22)$$

The factor two before the fraction comes from the upspin and downspin electrons entering into an energy level. This relation is reduced to

$$\frac{V}{3\pi^2} k_F^3 = N \quad (2.23)$$

where $V = L^3$ is the volume of the solid. Equation 2.20 affords $E_F = \frac{\hbar^2}{2m} k_F^2$. Through the use of this relation, k_F is eliminated.

$$E_F = \frac{\hbar^2}{2m} \left(\frac{3\pi^2 N}{V} \right)^{\frac{2}{3}} \quad (2.24)$$

This relation implies that E_F is determined by the electron density N/V . This equation is solved for N , and we obtain

$$N = \frac{V}{3\pi^2} \times \left(\frac{2mE_F}{\hbar^2} \right)^{\frac{3}{2}}. \quad (2.25)$$

When E is slightly increased by dE (Fig. 2.13), the electron number N increases by dN . The change is obtained by differentiating N by E .

$$D(E) = \frac{dN}{dE} = \frac{V}{2\pi^2} \left(\frac{2m}{\hbar^2} \right)^{\frac{3}{2}} E^{\frac{1}{2}} \quad (2.26)$$

From now on, the subscript F is omitted from E_F and k_F because the following relations hold more generally. $D(E)$ is the number of energy levels existing between E and dE , and called the **density of states**. Density of states in the three-dimensional free-electron model is proportional to \sqrt{E} (Fig. 2.13b). This plot looks like the parabola of $E(k)$ (Fig. 2.13a), but the horizontal axis represents a different quantity. The shaded region in Fig. 2.13b corresponds to the occupied region. In Fig. 2.13a, however, we cannot shade the region below E_F , because the occupied energy levels exist only on the energy band.

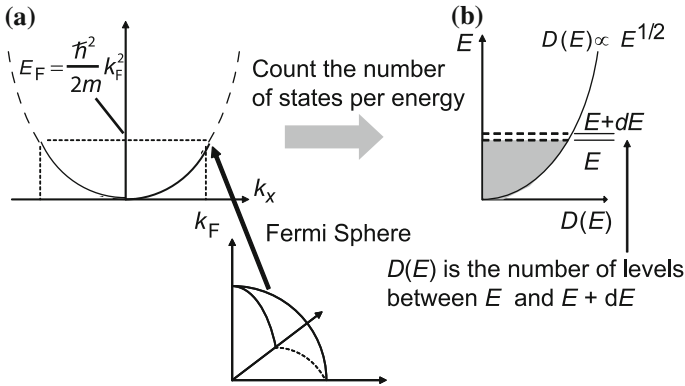


Fig. 2.13 Density of states $D(E)$ at the Fermi level

We shall extract the density of states in a different way. When the energy changes from E to $E + dE$ (Fig. 2.14), the spherical surface is $4\pi k^2$, and the volume of the spherical shell is $4\pi k^2 dk$. This is divided by $(\frac{2\pi}{L})^3$ to give

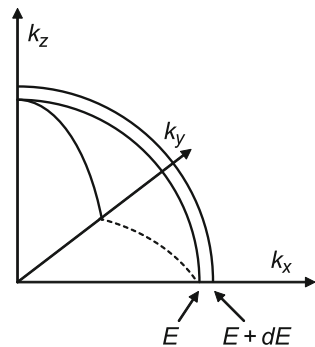
$$2 \frac{4\pi k^2 dk}{(\frac{2\pi}{L})^3} = dN. \tag{2.27}$$

$E = \frac{\hbar^2 k^2}{2m}$ gives $dE = \frac{\hbar^2 k}{m} dk$. These dN and dE are substituted in the definition of $D(E)$

$$D(E) = \frac{dN}{dE} = 2 \frac{4\pi k^2}{(\frac{2\pi}{L})^3} \frac{dk}{\frac{\hbar^2 k}{m}} = \frac{V}{2\pi^2} \frac{2m}{\hbar^2} k = \frac{V}{2\pi^2} \left(\frac{2m}{\hbar^2}\right)^{\frac{3}{2}} E^{\frac{1}{2}} \tag{2.28}$$

where $k = \left(\frac{2mE}{\hbar^2}\right)^{\frac{1}{2}}$ is used. This relation is identical to Eq. 2.26.

Fig. 2.14 Density of states at the Fermi spherical shell



Since the energy is represented by a parabola (Fig. 2.13a), the slope dE/dk increases with increasing E . Then, the number of states per energy decreases. However, the spherical surface increases in proportion to k^2 , and these two factors make $D(E)$ increase proportionally to \sqrt{E} . We will see that many important properties of metals such as specific heat (Sect. 2.3), conductivity (Sect. 3.1.3), and magnetic susceptibility (Sect. 4.4) increase in proportion to the density of states.

Example 2.2 Energy in a two-dimensional metal is given by $E = \frac{\hbar^2}{2m}(k_x^2 + k_y^2)$. Describe the shape of the Fermi surface. Calculate the density of states.

The Fermi surface of a two-dimensional metal is obtained by $k_x^2 + k_y^2 = k_F^2 = \text{constant}$, which gives a circle in the k_x - k_y plane. In the three-dimensional k -space, this gives an infinitely elongated cylinder (Fig. 2.15a). The number of the energy levels is calculated from the area of the circle πk^2 .

$$2 \frac{\pi k^2}{\left(\frac{2\pi}{L}\right)^2} = N \quad (2.29)$$

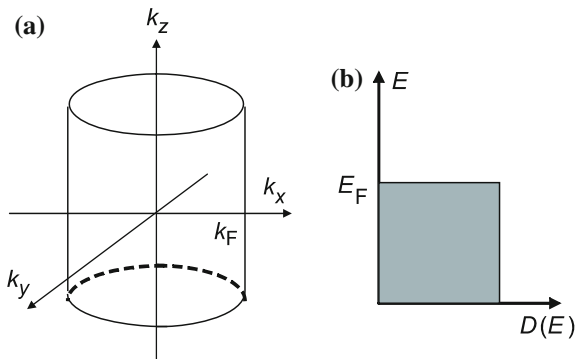
This is reduced to

$$N = \frac{L^2}{2\pi} k^2 = \frac{mL^2}{\hbar^2 \pi} E. \quad (2.30)$$

This is differentiated by E to give the density of states.

$$D(E) = \frac{dN}{dE} = \frac{mL^2}{\hbar^2 \pi} \quad (2.31)$$

Fig. 2.15 (a) Fermi surface and (b) density of states in a two-dimensional metal



The density of states of a two-dimensional metal does not depend on E (Fig. 2.15b).

Example 2.3 Energy in a one-dimensional metal is given by $E = \frac{\hbar^2}{2m} k_x^2$. Describe the shape of the Fermi surface. Calculate the density of states.

The Fermi surface of a one-dimensional metal is obtained by $k_x^2 = k_F^2 = \text{constant}$, which gives $k_x = \pm k_F$. In the three-dimensional k -space, this is a couple of planes (Fig. 2.15a), in which the $-k_F < k < k_F$ region is occupied, and the outside is unoccupied. The number of the energy levels is calculated from the length of the segment $2k_F$.

$$2 \frac{2k}{\frac{2\pi}{L}} = N \tag{2.32}$$

Since $E = \frac{\hbar^2 k^2}{2m}$ leads to $k = \frac{\sqrt{2mE}}{\hbar}$, k is deleted to give

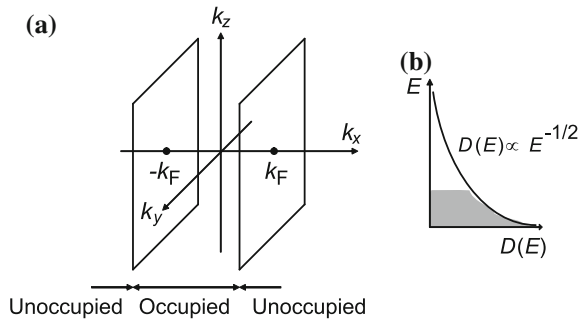
$$N = \frac{2L\sqrt{2mE}}{\pi\hbar} \tag{2.33}$$

which is differentiated by E to afford the density of states.

$$D(E) = \frac{dN}{dE} = \frac{L\sqrt{2m}}{\pi\hbar\sqrt{E}} \tag{2.34}$$

As shown in Fig. 2.16b, the density of states in a one-dimensional metal is proportional to $E^{-1/2}$, which diverges at the band edge ($E = 0$).

Fig. 2.16 (a) Fermi surface and (b) density of states in a one-dimensional metal



2.3 Fermi Distribution

An isolated molecule has discrete energy levels, whereas a solid has continuous energy bands. A solid consisting of a large number of atoms (N) has many energy levels, which are densely distributed with the energy interval proportional to $1/N$. In a molecule, energy levels below the HOMO are occupied, and those above the LUMO are unoccupied. In a solid, the energy bands below the Fermi energy are occupied. However, since the energy band is continuous, some energy levels are located only slightly above the Fermi energy, and some electrons are thermally excited to these energy levels (Fig. 2.17). This happens because the energy interval in the energy band is smaller than the thermal energy. Therefore, we have to consider a **distribution function** $f(E)$ representing the probability of the occupancy. $f(E)$ is one when 100 % occupied, and zero when entirely vacant. The distribution of metallic electrons is represented by the **Fermi-Dirac distribution function**. Here, we shall extract the Fermi-Dirac distribution function from statistical mechanics.

Suppose the number of energy levels with the same energy E is C_i . In the three-dimensional free-electron model, the C_i levels are located on the same spherical Fermi surface. Here, the states with different energies are labeled by the subscript i . Suppose N_i electrons are incorporated in these levels (Fig. 2.17). Since an electron is a Fermi particle, we cannot distinguish these N_i electrons. Then, N_i occupied states are chosen from the C_i states, and the statistical weight is

$$W_i = \frac{C_i!}{N_i!(C_i - N_i)!}. \quad (2.35)$$

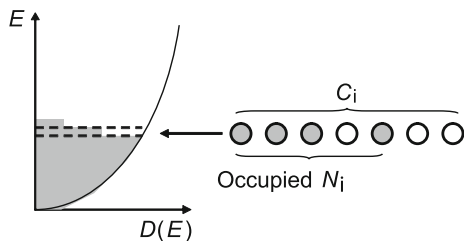
The entropy is obtained from the definition in statistical mechanics.

$$S = k_B \ln W = k_B \ln \prod_i W_i = k_B \sum_i \ln W_i = k_B \sum_i \ln \frac{C_i!}{N_i!(C_i - N_i)!} \quad (2.36)$$

This is simplified by using Stirling's approximation $\ln N! = N \ln N - N$.

$$S = k_B \sum_i (C_i \ln C_i - N_i \ln N_i - (C_i - N_i) \ln(C_i - N_i)). \quad (2.37)$$

Fig. 2.17 Fermi-Dirac distribution function



The Gibbs free energy is represented by $F = E - TS - \mu N$, where μ is the chemical potential. Note that the total energy is $E = \sum N_i E_i$ and the total electron number is $N = \sum N_i$. Here, the distribution of N_i which minimizes F is realized. This is obtained by placing the N_i derivative of F to be zero.

$$\frac{\partial F}{\partial N_i} = E_i + k_B T (\ln N_i - \ln(C_i - N_i)) - \mu = 0 \tag{2.38}$$

This leads to

$$\frac{C_i - N_i}{N_i} = e^{\frac{E_i - \mu}{k_B T}}. \tag{2.39}$$

As shown in Fig. 2.18, the distribution function corresponds to $f(E) = N_i/C_i$. This is obtained from the above equation.

$$f(E_i) = \frac{N_i}{C_i} = \frac{1}{e^{\frac{E_i - \mu}{k_B T}} + 1} \tag{2.40}$$

This is the Fermi distribution function. In this notation, the density of states is $D(E) = C_i$, and the distribution function is $f(E) = N_i/C_i$. Then, as shown in Fig. 2.18, $D(E) \times f(E)$ gives the electron number N_i .

The Fermi distribution function is depicted in Fig. 2.19. At $T = 0$ K, Eq. 2.40 gives

$$\begin{aligned} f(E) &= \frac{1}{e^{-\infty} + 1} = 1 \quad \text{for } E < \mu \\ f(E) &= \frac{1}{e^{+\infty} + 1} = 0 \quad \text{for } E > \mu \end{aligned} \tag{2.41}$$

which affords a step function (Fig. 2.19). At a finite temperature, $e^{\frac{E-\mu}{k_B T}}$ changes gradually, and $f(E)$ drops smoothly (Fig. 2.19). At $E = \mu$, $f(E)$ is always 1/2. Since

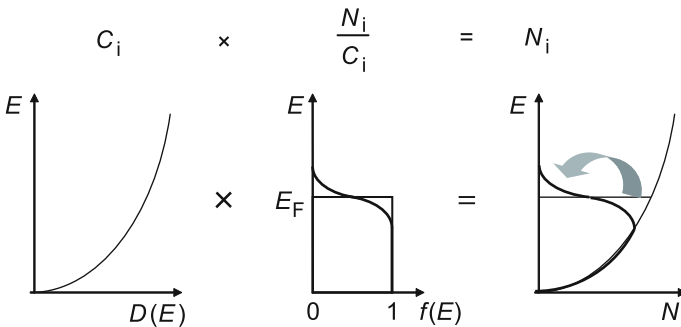
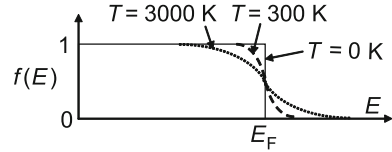


Fig. 2.18 Density of states \times Distribution function = Number of electrons

Fig. 2.19 Fermi distribution functions at finite temperatures



$e^{\frac{E-\mu}{k_B T}}$ changes only around the $E \sim \mu \pm k_B T$ region, $f(E)$ is mostly either one or zero except for the very neighbor of $E \sim \mu$. μ of an inorganic metal is in the same order as the bandwidth, which is as large as $5 \text{ eV} \sim 50,000 \text{ K}$. At 300 K , the step is smoothed in the small region of $300 \text{ K}/50,000 \text{ K} \sim 0.6 \%$, and the excited electrons are less than 1% of the total electrons.

In order to demonstrate this point more clearly, we shall calculate the specific heat of metallic electrons. Since the electron number is represented by $D(E)f(E)$ (Fig. 2.18), the internal energy is obtained by multiplying E to the electron number.

$$U(T) = \int_0^{\infty} (E - E_F) D(E) f(E) dE \quad (2.42)$$

Here, $E - E_F$ instead of E is multiplied in order to adopt E_F as the standard. The specific heat at constant volume is obtained by differentiating the internal energy by temperature.

$$C_V = \frac{\partial U}{\partial T} = \int_0^{\infty} (E - E_F) D(E) \frac{\partial f(E)}{\partial T} dE \quad (2.43)$$

Note that T appears only in $f(E)$. The T derivative of $f(E)$ is obtained by using $x = \frac{E-\mu}{k_B T}$ in

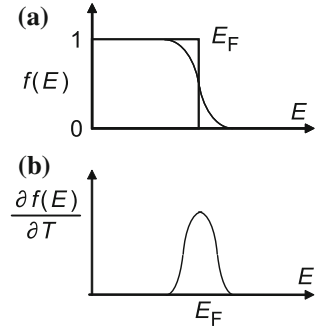
$$f(E_i) = \frac{1}{e^{\frac{E_i-\mu}{k_B T}} + 1} = \frac{1}{e^x + 1}. \quad (2.44)$$

This affords

$$\frac{\partial f}{\partial T} = \frac{E - \mu}{k_B T^2} \frac{e^x}{(e^x + 1)^2}. \quad (2.45)$$

Since $f(E)$ is either one or zero except for the neighbor of $E \sim \mu$, the derivative is mostly zero. This function is only non zero around the neighbor of E_F (Fig. 2.20b).

Fig. 2.20 (a) Fermi distribution function and (b) the derivative



The integral in Eq. 2.43 is finite only around E_F , and $D(E)$ is approximated by $D(E_F)$. Then, $D(E_F)$ is taken out of the integral to afford

$$\begin{aligned}
 C_V &= D(E_F) \int_0^{\infty} (E - E_F) \frac{\partial f(E)}{\partial T} dE = D(E_F) \int_0^{\infty} (k_B T x) \frac{x}{T} \frac{e^x}{(e^x + 1)^2} k_B T dx \\
 &= k_B^2 T D(E_F) \int_0^{\infty} x^2 \frac{e^x}{(e^x + 1)^2} dx.
 \end{aligned} \tag{2.46}$$

Since this integral is $\pi^{2/3}$, the specific heat is

$$C_V = \frac{\pi^2}{3} D(E_F) k_B^2 T. \tag{2.47}$$

The specific heat is proportional to T , and represented as $C_v = \gamma T$. The coefficient $\gamma = \frac{\pi^2}{3} D(E_F) k_B^2$ contains only $D(E_F)$ as a characteristic property of a material. As another notation, the density of states in a three-dimensional metal is obtained from Eq. 2.25 as

$$D(E_F) = \frac{3 N}{2 E_F} = \frac{3 N}{2 k_B T_F} \tag{2.48}$$

so the specific heat is

$$C_v = \frac{\pi^2}{3} \frac{3 N}{2 k_B T_F} k_B^2 T = \frac{\pi^2}{2} N k_B \frac{T}{T_F} = \frac{\pi^2}{2} n R \frac{T}{T_F}. \tag{2.49}$$

Here, the **Fermi temperature** T_F is defined by $E_F = k_B T_F$. This is in the order of 50,000 K, implying only $T/T_F \sim 300 \text{ K}/50,000 \text{ K} \sim 0.6 \%$ electrons are thermally excited. If electrons follow the classical distribution instead of the Fermi distribution, the electron specific heat should be $C_v \sim 3R$ according to **Dulong–Petit’s law**, where R is the gas constant and the number three appears from the $x, y,$

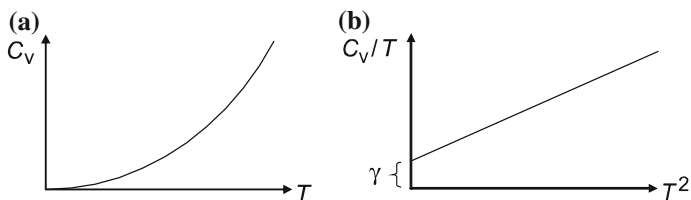


Fig. 2.21 Temperature dependence of low-temperature specific heat at low temperatures

and z directions. Equation 2.49 becomes less than 1 % of this value because the electrons are Fermi particles, reflecting the quantum mechanical nature of the metal electrons. The states below E_F are occupied and those above E_F are unoccupied, and this situation is practically unchanged at a finite temperature. Then, the Fermi surface is obscured only very slightly by the thermal excitation. Even the metal electrons are occupied similarly to the ordinary molecular orbitals, where the states below the HOMO are occupied, and those above the LUMO are unoccupied.

When the electron-specific heat is added to the lattice-specific heat from the thermal vibration following T^3 (Fig. 2.21a), we obtain

$$C_v = \gamma T + \beta T^3. \quad (2.50)$$

This is divided by T to lead to

$$C_v/T = \gamma + \beta T^2 \quad (2.51)$$

so the plot of C_v/T versus T^2 gives a straight line (Fig. 2.21b). The intercept of this plot affords γ . The second term βT^3 is overwhelming at high temperatures, but becomes small at liquid helium temperatures, where the γT term is more important. Then, low-temperature specific heat measurement below liquid helium temperatures gives γ from the plot like Fig. 2.21b. Since γ is determined only from $D(E_F)$ (Eq. 2.47), this affords an estimation of $D(E_F)$. In an insulator having no metallic electrons, a similar plot affords a straight line passing zero.

Example 2.4 In **Bose–Einstein statistics**, each state can be occupied by more than two particles. In this condition, we shall consider a case where N_i particles enter the C_i states with the same energy. Figure 2.22 represents an example in which these states are occupied by 3, 1, 2, 0, 2 ... particles. Suppose the white balls represent the borders between the states, and the black balls are particles incorporated as 3, 1, 2, 0, 2 ... The statistical weight is given by the orders of N_i black balls and $C_i - 1$ white balls.

$$W_i = \frac{(C_i + N_i - 1)!}{N_i!(C_i - 1)!} \tag{2.52}$$

From this relation, calculate the Bose–Einstein distribution by minimizing the free energy. For simplicity, replace $C_i - 1$ with C_i .

Assuming $C_i - 1 \rightarrow C_i$, and using Stirling’s approximation, we obtain

$$\ln W_i = (C_i + N_i) \ln(C_i + N_i) - N_i \ln N_i - C_i \ln C_i. \tag{2.53}$$

This is substituted in $F = E - TS - \mu N$, and differentiated by N_i to give

$$\frac{\partial F}{\partial N_i} = E_i + k_B T (\ln(N_i + C_i) - \ln N_i) - \mu = 0. \tag{2.54}$$

This gives

$$\frac{C_i + N_i}{N_i} = \exp\left(\frac{E_i - \mu}{k_B T}\right). \tag{2.55}$$

The distribution function is

$$f(E_i) = \frac{N_i}{C_i} = \frac{1}{\exp\left(\frac{E_i - \mu}{k_B T}\right) - 1}. \tag{2.56}$$

At $T = 0$ K, this equation leads to

$$f(E) = \frac{1}{e^{+\infty} - 1} = 0 \quad \text{for } E > \mu$$

$$e^0 = 1 \text{ affords } f(E) \rightarrow \infty \quad \text{for } E = \mu \tag{2.57}$$

and all particles fall into the lowest state (Fig. 2.23). This situation is called the Bose–Einstein condensation.

Fig. 2.22 Bose distribution

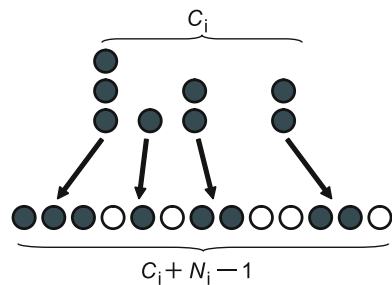
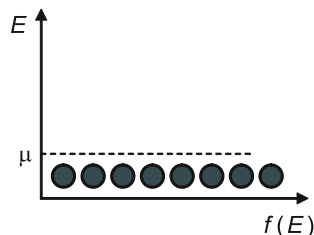


Fig. 2.23 Bose-Einstein condensation at $T = 0$ K



When $E_i - \mu$ is replaced by $\hbar\omega$ in Eq. 2.56, the Planck distribution

$$f(\omega) = \frac{1}{\exp\left(\frac{\hbar\omega}{k_B T}\right) - 1} \quad (2.58)$$

is obtained. Since a photon is a Bose particle, the black body radiation (Sect. 1.1) follows the Planck distribution. A phonon is a representation of the lattice vibration, which is another Bose particle. The lattice vibration also follows this relation.

In quantum statistical mechanics, the Fermi particles are particles with half-integer spins. The examples are electrons, protons, neutrons, and ^3He . These particles follow the Fermi distribution. The Bose particles are particles with integer spins. The examples are photons, phonons, and ^4He . These particles follow the Bose distribution. These distributions are generally represented by

$$f(E_i) = \frac{1}{\exp\left(\frac{E_i - \mu}{k_B T}\right) \pm 1} \quad (2.59)$$

where the + sign gives the Fermi distribution, and the - sign gives the Bose distribution. In the large energy limit ($E - \mu \gg k_B T$), the exponential is larger than one, and ± 1 is neglected to give the classical **Boltzmann distribution**.

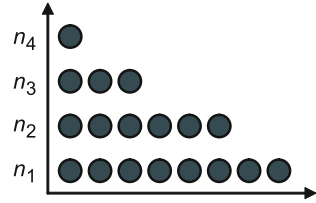
$$f(E_i) = \exp\left(-\frac{E_i - \mu}{k_B T}\right) \quad (2.60)$$

Example 2.5 In the classical Boltzmann distribution, n_i particles of the total $N = \sum n_i$ particles are distributed into the i -th state. The statistical weight is (Fig. 2.24)

$$W = \frac{N!}{n_1! n_2! n_3! \dots} \quad (2.61)$$

From this relation, calculate the Boltzmann distribution by minimizing the free energy.

Fig. 2.24 Boltzmann distribution



Stirling’s approximation affords

$$\ln W = \ln \frac{N!}{n_1!n_2!n_3!\dots} = N \ln N - \sum_i n_i \ln n_i. \tag{2.62}$$

This is placed in $F = E - TS - \mu N$ to give

$$F = \sum_i E_i n_i - k_B T \left(N \ln N - \sum_i n_i \ln n_i \right) - \mu \sum_i n_i. \tag{2.63}$$

This is differentiated by n_i and equated zero to afford

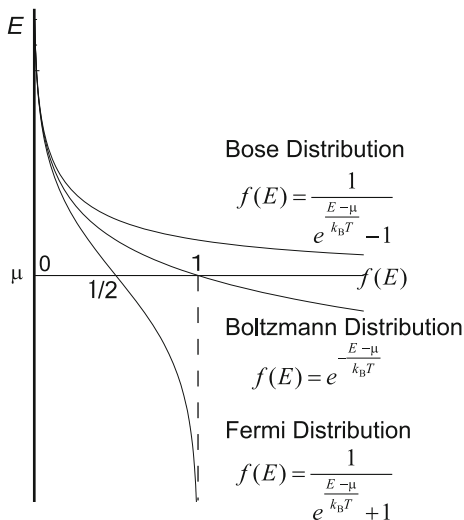
$$\frac{\partial F}{\partial n_i} = E_i + k_B T (\ln n_i + 1) - \mu = 0. \tag{2.64}$$

This gives the Boltzmann distribution.

$$f(E_i) = n_i = \exp\left(-\frac{E_i - \mu}{k_B T}\right) \tag{2.65}$$

The Fermi, Bose, and Boltzmann distributions are summarized in Fig. 2.25. At $T = 0$ K, the Fermi distribution is step-like, and in the Bose distribution all particles condense into the $E = \mu$ state. These ground states appear, respectively, when a state is occupied only by a single particle, and by multiple particles. At $E - \mu \gg k_B T$, the exponential becomes much larger than one, and all distributions converge to the classical Boltzmann distribution.

Fig. 2.25 Various kinds of distributions



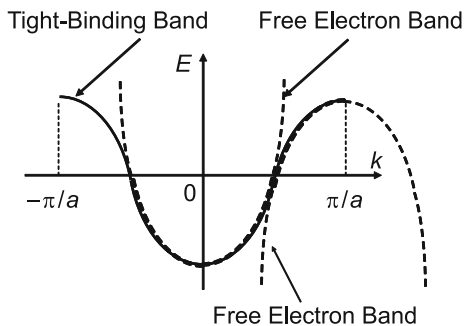
2.4 Relation Between the Tight-Binding Approximation and the Free-Electron Model

The tight-binding and the free-electron models are two different views of solid electrons. We can expand the tight-binding energy band (Eq. 2.7) around $k = 0$.

$$E(k) = E(0) + bk^2 + \dots \quad (2.66)$$

Here, the k -linear term for the cosine function is zero. When bk^2 is regarded as $\frac{\hbar^2 k^2}{2m^*}$, the free-electron model is an approximation of the tight-binding band (Fig. 2.26). Therefore, the **effective mass** $\frac{1}{m^*} = \frac{1}{\hbar^2} \frac{\partial^2 E(k)}{\partial k^2}$ is not equal to the electron mass.

Fig. 2.26 Relation between the tight-binding and free electron models



Example 2.6 Calculate the relation of the effective mass m^* in the free-electron model to β in the tight-binding approximation.

Equation 2.7 is differentiated by k twice.

$$\begin{aligned} \frac{\partial E}{\partial k} &= -2\beta a \sin ka \\ \frac{\partial^2 E}{\partial k^2} &= -2\beta a^2 \cos ka. \end{aligned} \tag{2.67}$$

This is substituted in the definition of the effective mass $\frac{1}{m^*} = \frac{1}{\hbar^2} \frac{\partial^2 E(k)}{\partial k^2}$, and k is assumed to be zero.

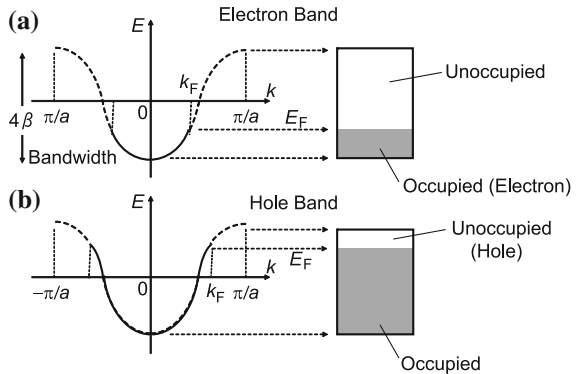
$$m^* = -\frac{\hbar^2}{2\beta a^2 \cos ka} \rightarrow -\frac{\hbar^2}{2\beta a^2} \tag{2.68}$$

The resonance integral β in the molecular orbital theory is called a **transfer integral** in solid-state physics, and represented by t . Then, Eq. 2.7 is rewritten as

$$E = \alpha + 2t \cos ka. \tag{2.69}$$

As shown in Fig. 2.26, the difference between the tight-binding band and the free-electron model increases at large k . In particular, the free-electron band increases without a limit, whereas the tight-binding band reaches to a limit at $k = \pi/a$. A free-electron band does not have a bandwidth. However, we can expand the tight-binding band at $k = \pi/a$, and a downward parabola is obtained (Fig. 2.26). Here, $b < 0$ leads to $m^* < 0$, indicating the existence of holes with positive charges. Accordingly, the lower half band is approximated by electrons, while the upper half band has holes (Fig. 2.27).

Fig. 2.27 (a) Electron band and (b) hole band



Example 2.7 Calculate the density of states at the band center (in the half-filled case) of a one-dimensional tight-binding band with the bandwidth 1 eV.

Equation 2.67 leads to

$$D(E) = \frac{\partial N}{\partial E} = \frac{\partial N}{\partial k} \frac{\partial k}{\partial E} = -\frac{a}{2\pi} \frac{1}{2\beta a \sin ka} = -\frac{1}{4\beta\pi \sin ka}.$$

Here, $\sin ka$ is one at the band center, so $4\beta = 1$ eV affords $D(E) = 1/\pi = 0.318$ states/eV. This is minimum in the band, and $D(E)$ increases and diverges towards the band edge similarly to the one-dimensional free-electron band (Example 2.3).

2.5 Two-Dimensional Energy Band

Next, we shall investigate the two-dimensional tight-binding band. As shown in Fig. 2.28, consider a square lattice with a transfer integral β between the neighboring atoms. Similarly to Eq. 2.3, a crystal orbital that satisfies the Bloch condition is represented by

$$\psi = \sum_n \sum_m e^{ik_x a} e^{ik_y a} \chi_{nm}. \quad (2.70)$$

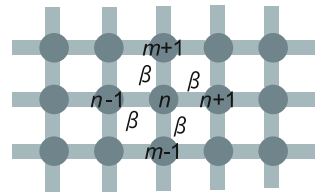
This is substituted in Eq. 2.4 to give the energy.

$$E \propto \sum_n \sum_m \sum_p \sum_q e^{i(n-p)k_x a} e^{i(m-q)k_y a} \int \chi_{np}^* H \chi_{mq} d\tau \quad (2.71)$$

For a given (n, m) , nonzero integrals are $\beta e^{ik_x a}$ for $(p, q) = (n-1, m)$, α for (n, m) , $\beta e^{-ik_x a}$ for $(n+1, m)$, $\beta e^{ik_y a}$ for $(n, m-1)$, and $\beta e^{-ik_y a}$ for $(n, m+1)$. These terms are collected to

$$E \propto e^{ik_x a} \beta + \alpha + e^{-ik_x a} \beta + e^{ik_y a} \beta + e^{-ik_y a} \beta. \quad (2.72)$$

Fig. 2.28 Two-dimensional square lattice



This affords

$$E = \alpha + 2\beta \cos k_x a + 2\beta \cos k_y a. \tag{2.73}$$

We consider the range of k to be $-\pi/a < k_x < \pi/a$ and $-\pi/a < k_y < \pi/a$, so the first Brillouin zone is represented by a square shown in Fig. 2.29a. Energy given by Eq. 2.73 is depicted in Fig. 2.29b. Energy at the representative points in the k space is

$$\begin{aligned} (k_x, k_y) = (0, 0) & \quad \alpha + 4\beta \\ (\pi/a, 0) & \quad \alpha \\ (0, \pi/a) & \quad \alpha \\ (\pi/a, \pi/a) & \quad \alpha - 4\beta. \end{aligned}$$

The minimum energy is $\alpha + 4\beta$, and the maximum energy is $\alpha - 4\beta$, so the bandwidth is $8|\beta|$. The bandwidth is generally given as $2z|\beta|$, where z is the number of the neighboring atoms (coordination number). In a one-dimensional band, $z = 2$ affords $4|\beta|$. In the present two-dimensional square lattice, $z = 4$ affords $8|\beta|$. Similarly, the tight-binding energy of a three-dimensional cubic lattice is

$$E = \alpha + 2\beta \cos k_x a + 2\beta \cos k_y a + 2\beta \cos k_z a. \tag{2.74}$$

This affords the bandwidth $12|\beta|$.

Suppose the two-dimensional square band is half-filled. The Fermi energy is $E_F = \alpha$, and the Fermi surface is a square shown in Fig. 2.30. It seems surprising that the Fermi surface is surrounded by straight lines, but applying the sum equation of cosine functions to Eq. 2.73, we obtain the straight lines because the sine becomes zero at $\pm k_x \pm k_y = \pi/a$. Inside of the square is occupied, whereas the outside squares are unoccupied. The outside squares in Fig. 2.30b are regarded as hole pockets.

Copper-oxide high-temperature superconductors have a CuO square lattice (Fig. 2.31a). The copper atoms are octahedrally coordinated, and oxygen atoms exist in between the Cu atoms. The axial interaction is less important, so the CuO network is regarded as a square lattice. The Fermi energy is located in the Cu $d_{x^2-y^2}$

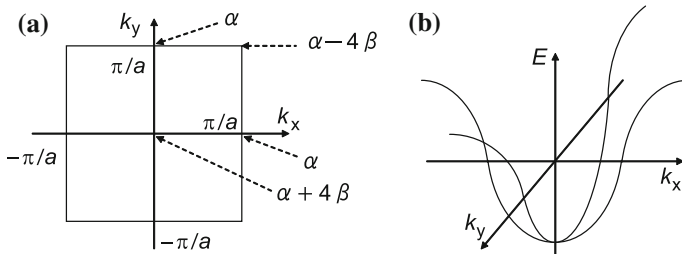


Fig. 2.29 (a) First Brillouin zone and (b) energy band in the two-dimensional square lattice

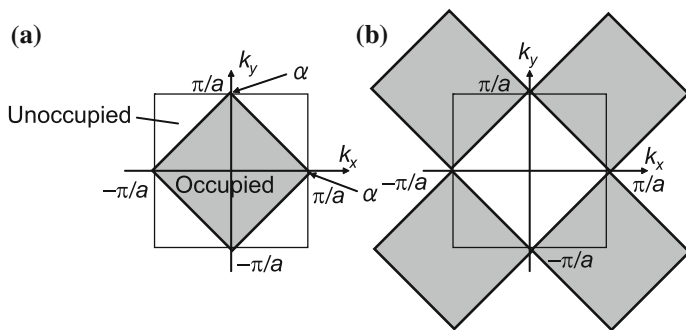
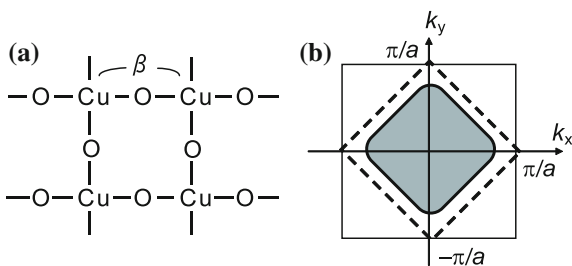


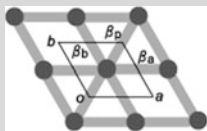
Fig. 2.30 Fermi surface in the half-filled two-dimensional square lattice

Fig. 2.31 (a) Structure and (b) Fermi surface of a copper oxide superconductor



band represented by Eq. 2.73. The non superconducting parent compound La_2CuO_4 has Cu^{2+} and the Cu $d_{x^2-y^2}$ band is half-filled. The Fermi surface is represented by Fig. 2.30, and this compound is a Mott insulator (Chap. 5). Superconductors have such compositions as $(\text{La}_{1-x}\text{Sr}_x)_2\text{CuO}_4$; because Sr^{2+} has a smaller charge than La^{3+} , Cu^{2+} is partly converted to Cu^{3+} . This compound has less electrons than the parent compound, and the CuO network is hole doped. The resulting superconducting material has smaller (electron) Fermi surface than that of the parent compound (Fig. 2.31b), and shows metallic conductivity.

Example 2.8 Calculate the energy band of a triangular lattice, in which the three directions have different transfers, β_a , β_b , and β_p . Calculate the bandwidth.



The atomic orbital in a unit cell is one, and the transfers are β_a for $\pm a$, β_b for $\pm b$, and β_p for $\pm(a + b)$. Since the neighboring atoms are six, the energy band is obtained similarly to Eq. 2.72.

$$\begin{aligned}
 E &= \alpha + \beta_a e^{ik_a a} + \beta_a e^{-ik_a a} + \beta_b e^{ik_b b} + \beta_b e^{-ik_b b} + \beta_p e^{i(k_a a + k_b b)} + \beta_p e^{-i(k_a a + k_b b)} \\
 &= \alpha + 2\beta_a \cos k_a a + 2\beta_b \cos k_b b + 2\beta_p \cos(k_a a + k_b b)
 \end{aligned}$$

Since each cosine function changes over the ± 1 range, the bandwidth is $4|\beta_a| + 4|\beta_b| + 4|\beta_p|$.

2.6 Tight-Binding Approximation for General Crystals

We shall consider a unit cell which contains more than two atoms. For example, a unit cell in Fig. 2.32 involves two atoms, 1 and 2. In analogy with the LCAO in the molecular orbital theory, the whole orbital is represented by using the atomic orbitals χ_1 and χ_2

$$\psi = \sum_{i=1}^2 c_i \chi_i \quad (2.75)$$

where $i = 1$ and 2 . In order to take account of χ_i involved in different cells, χ_i is replaced by the crystal orbital.

$$\chi_i \rightarrow \sum_n^N e^{ink_a} \chi_i(n). \quad (2.76)$$

Combining Eqs. 2.75 and 2.76, we obtain

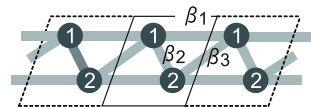
$$\psi = \sum_{i=1}^2 \sum_n^N c_i e^{ink_a} \chi_i(n). \quad (2.77)$$

In general, i is a sum for orbitals in a unit cell, and n is a sum for different cells.

Similarly, to the usual molecular orbital theory, the energy is obtained by using this equation in Eq. 2.4. The resulting equation contains c_1 and c_2 , so we calculate $\frac{\partial E}{\partial c_i} = 0$, leading to the secular equation.

$$\begin{vmatrix} \alpha_{11}(k) - E & \beta_{12}(k) \\ \beta_{21}(k) & \alpha_{22}(k) - E \end{vmatrix} = 0 \quad (2.78)$$

Fig. 2.32 Two atoms in a unit cell



The diagonal term $\alpha_{ii}(k)$ is an integral where the Hamiltonian is sandwiched by the same crystal orbital $\sum e^{inka} \chi_i(n)$

$$\begin{aligned} \alpha_{ii}(k) &= \int \left(\sum_m e^{-imka} \chi_i^*(m) \right) H \left(\sum_n e^{inka} \chi_i(n) \right) d\tau \\ &= \alpha_i + \sum_{n'} \beta_{ii}(n') e^{in'ka}. \end{aligned} \quad (2.79)$$

which includes not only α_i coming from the same χ_i in the same unit cell, but also $\beta_{ii}(k)$ coming from different χ_i belonging to the neighboring cells. The latter is k dependent. For example, atom 1 in Fig. 2.32 includes β_1 to the neighboring cells.

$$\alpha_{11} = \alpha_1 + \beta_1 e^{ika} + \beta_1 e^{-ika} = \alpha_1 + 2\beta_1 \cos ka \quad (2.80)$$

The nondiagonal term is similarly obtained.

$$\begin{aligned} \beta_{ij}(k) &= \int \left(\sum_m e^{-imka} \chi_i^*(m) \right) H \left(\sum_n e^{inka} \chi_j(n) \right) d\tau \\ &= \sum_n \beta_{ij}(n') e^{in'ka} \end{aligned} \quad (2.81)$$

For example, the term 12 in Fig. 2.31 is

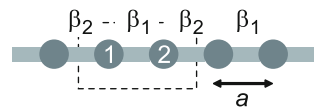
$$\beta_{12} = \beta_2 + \beta_3 e^{-ika}. \quad (2.82)$$

This consists of the intra-cell β_2 and the inter-cell β_3 multiplied by e^{-ika} . In general, when the transfer β exists in the r direction between the atoms 1 and 2, the matrix element is obtained by summing βe^{ikr} . The following example illustrates a practical case.

Example 2.9 Calculate the energy band of a one-dimensional alternating chain, where β is alternately β_1 and β_2 as shown in Fig. 2.33. Estimate the overall bandwidth and the energy gap.

A unit cell contains two atoms (1 and 2), so the secular equation is 2×2 , where the diagonal terms are $\int \chi_1^* H \chi_1 d\tau = \int \chi_2^* H \chi_2 d\tau = \alpha$ and the nondiagonal terms are $\beta_1 + \beta_2 e^{i2ka}$ and $\beta_1 + \beta_2 e^{-i2ka}$.

Fig. 2.33 One-dimensional alternating chain



The secular equation is

$$\begin{vmatrix} \alpha - E & \beta_1 + \beta_2 e^{i2ka} \\ \beta_1 + \beta_2 e^{-i2ka} & \alpha - E \end{vmatrix} = 0. \quad (2.83)$$

This is reduced to

$$(\alpha - E)^2 = (\beta_1 + \beta_2 e^{i2ka})(\beta_1 + \beta_2 e^{-i2ka}) \quad (2.84)$$

which gives

$$E = \alpha \pm \sqrt{\beta_1^2 + \beta_2^2 + 2\beta_1\beta_2 \cos 2ka}. \quad (2.85)$$

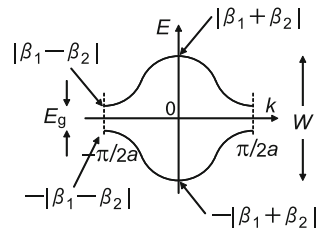
This is depicted in Fig. 2.34. Since the energy at $k = 0$ is $E = \pm|\beta_1 + \beta_2|$, the overall bandwidth is $W = 2|\beta_1 + \beta_2|$. The energy at $k = \pi/a$ is $E = \pm|\beta_1 - \beta_2|$, so the energy gap is $E_g = 2|\beta_1 - \beta_2|$.

When we assume $\beta_1 = \beta_2 = \beta$ in Eq. 2.85, we obtain

$$\begin{aligned} E &= \alpha \pm \sqrt{\beta^2 + \beta^2 + 2\beta^2 \cos 2ka} = \alpha \pm \beta\sqrt{2(1 + \cos 2ka)} \\ &= \alpha + 2\beta \cos ka. \end{aligned} \quad (2.86)$$

Here, we used the double-angle formula, $1 + \cos 2x = 2 \cos^2 x$. This is identical to Eq. 2.7. When $\beta_1 = \beta_2$, the energy gap $2|\beta_1 - \beta_2|$ is zero, and the upper and the lower bands are connected (Fig. 2.35a). We have defined the unit cell as $2a$ (Fig. 2.33), so the uniform chain has a periodicity of a . When the upper band is moved to the $k > \pi/2a$ region, the band is depicted in the $-\pi/a < k < \pi/a$ region (Fig. 2.25b). This is the original cosine band. The band scheme like (a) is called a **reduced zone**, and the scheme (b) is called an **extended zone**. These two represent the same band. The energy band at $\beta_1 \neq \beta_2$ is depicted (c) in the reduced zone and (d) in the extended zone. If this band is half-filled, the lower band is fully occupied, but the upper band is empty. Figure 2.35a is equivalent to Fig. 2.5a, where polyacetylene is a metal. In the actual polyacetylene, the single and double bonds have different $\beta_1 \neq \beta_2$ (bond alternation), and an energy gap emerges as shown in Fig. 2.35c, d. Note the lattice periodicity is doubled in this case.

Fig. 2.34 Energy band in a one-dimensional alternating chain



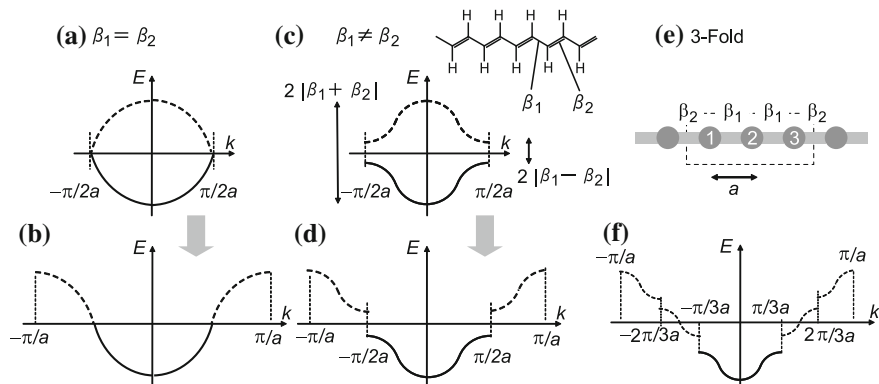


Fig. 2.35 (a, b) Uniform one-dimensional band and (c, d) alternating one-dimensional band. (e) Three-fold chain and (f) the energy band

Similarly, when the periodicity of the chain is $3a$ (Fig. 2.35e), energy gaps appear at $k = \pi/3a$ as show in Fig. 2.35f. Figure 2.35e has only two kinds of β_1 and β_2 , but the periodicity $\beta_1\beta_1\beta_2$ is three-fold. In general, when the lattice periodicity is n times the original lattice, the repeating unit in the k space becomes $1/n$, and an energy gap emerges at π/na . When k_F is located at π/na , the material becomes an insulator. Consequently, a $1/n$ -filled one-dimensional band becomes insulating when the lattice periodicity becomes na . This is called the **Peierls transition**. Polyacetylene is regarded as a Peierls insulator. Bond alternation in antiaromatic cyclobutadiene (Example 1.12) is also regarded as a Peierls insulator. In Chap. 7, we discuss organic conductors with noninteger periodicity such as 3.39 molecules (Fig. 7.14) and 2.29 molecules (Fig. 7.43). Even in these cases, a gap appears at k_F corresponding to the inverse of the periodicity.

In general, when a unit cell contains N atomic orbitals, the LCAO of the crystal orbital leads to a secular equation

$$\begin{vmatrix} \alpha_{11}(k) - E & \beta_{12}(k) & \dots \\ \beta_{21}(k) & \alpha_{22}(k) - E & \dots \\ \vdots & \vdots & \ddots \end{vmatrix} = 0. \quad (2.87)$$

The matrix elements depend on $\mathbf{k} = (k_x, k_y, k_z)$. At a certain \mathbf{k} , however, the matrix elements are complex numbers, and the solution gives N energy levels. Note the solutions are real numbers because the matrix is a Hermetian. When we use a slightly different \mathbf{k} , we obtain slightly different matrix elements. The energy levels are slightly different. By connecting these energy levels, we obtain the energy bands (Fig. 2.36). Even when N is very large, the number of the energy bands is the same as the number of the starting orbitals N .

Figure 2.36 is the energy bands of germanium. Germanium forms a diamond lattice from the Ge-Ge covalent bonds, where the original $4s4p^3$ atomic orbitals construct the bonding and antibonding orbitals. The occupied bonding orbitals form

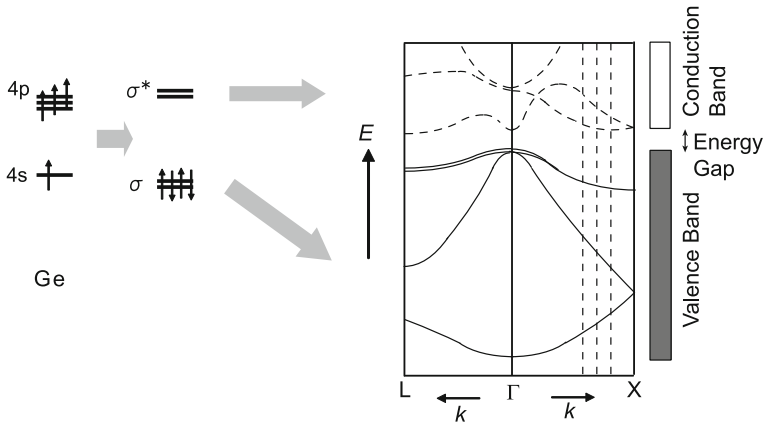


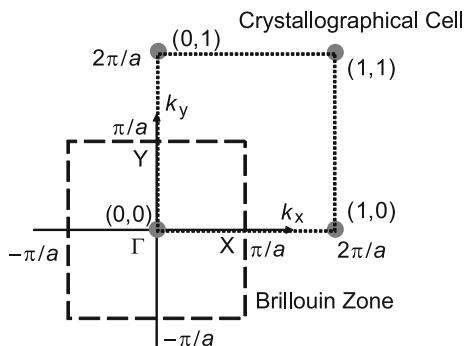
Fig. 2.36 An example of a three-dimensional energy band: chemical bonds and energy bands in germanium

the valence band, and the unoccupied antibonding orbitals form the conduction band. An energy gap emerges between the valence and conduction bands, so germanium is a semiconductor. The energy gap is 0.66 eV for germanium, which increases to 1.12 eV in silicon and 5.47 eV in diamond.

2.7 Brillouin Zone

The unit cell in the k space is called the Brillouin zone. The Brillouin zone of the two-dimensional square lattice (Sect. 2.5) is shown in Fig. 2.37. In crystallography, lattice points in the inverse space are located on the points such as (1, 0) and (0, 1). In solid-state physics, these points are on $2\pi/a$, and regarded as equivalent to the origin Γ , when we discuss the electronic state. In solid-state physics, the Fourier transform is defined by e^{ikr} , so the lattice point appears at $2\pi/a$. In contrast, the

Fig. 2.37 The first Brillouin zone (dashed) and the crystallographical cell (dotted) in the two-dimensional square lattice



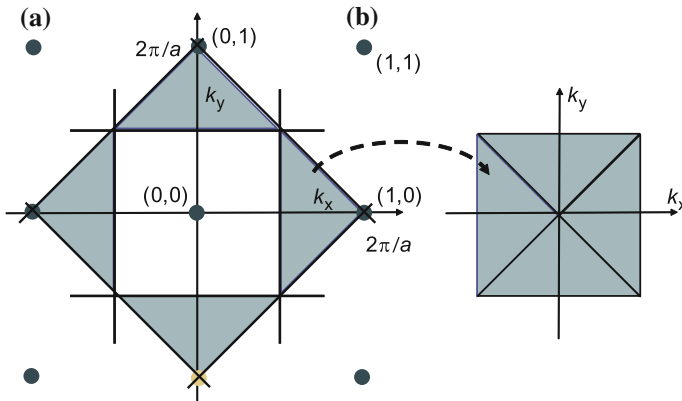


Fig. 2.38 The second Brillouin zone in the two-dimensional square lattice

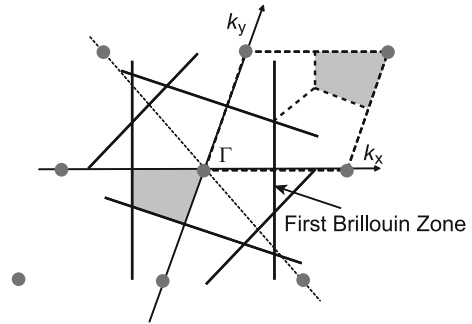
Fourier transform in crystallography is defined by $e^{2\pi i k r}$, and the lattice point is located on $k = 1/a$. Note the definition of the k space is different by 2π .

The boundary of the Brillouin zone is defined by the midpoint to the adjacent lattice point. Therefore, the boundary appears at π/a . In general, the zone boundary is obtained by the perpendicular bisector between the original and adjacent lattice points. The resulting Brillouin zone is a square (Fig. 2.37). A crystallographical unit cell is surrounded by the lattice points, which is different from the Brillouin zone (Fig. 2.37). However, these two squares have the same area, and represent the equivalent unit cell. The origin of the Brillouin zone $(0, 0)$ is conventionally called the Γ point, and the crossing points of the k_x and k_y axes to the zone boundary are, respectively, called the X and Y points.

Since the Brillouin zone is surrounded by perpendicular bisectors to the adjacent lattice points, the perpendicular bisector to the $(1, 1)$ point defines an oblique boarder (Fig. 2.38). Accordingly, shaded regions surrounded by the new perpendicular bisectors are generated out of the first Brillouin zone. The right triangle is located left of the $(1, 0)$ point, so moved to the left of the $(0, 0)$ point. Similarly, the left triangle is moved to the right and so on to generate a new square that is identical to the first Brillouin zone. This square is a region originally located out of the first Brillouin zone, and called the second Brillouin zone. In the same way, perpendicular bisectors to more distant lattice points define the third and fourth Brillouin zones.

Next, we investigate non orthogonal lattices. As shown in Fig. 2.39, the perpendicular bisectors define an irregular hexagon, which is the first Brillouin zone. In an oblique lattice, perpendicular bisectors to diagonal lattice points constitute the boarder. In crystallography, a unit cell is a parallelogram, but for example, the

Fig. 2.39 The Brillouin zone for a non orthogonal lattice



shaded regions in Fig. 2.39 are equivalent to each other. We can construct the first Brillouin zone by moving four separate panels from the parallelogram.

Examples of three-dimensional Brillouin zones are shown in Fig. 2.40. Brillouin zones of primitive cubic and orthorhombic lattices are again primitive cubic and orthorhombic lattices (Fig. 2.40b), because the lattice is orthogonal. However, similar to Fig. 2.39, a C-center orthogonal system leads to a hexagonal face (Fig. 2.40c). The reciprocal cell of a body-center cubic lattice is a face-center cubic, and that of a face-center cubic lattice is a body-center cubic. The corresponding Brillouin zones are shown in Fig. 2.40d, e. The polyhedron in Fig. 2.40d is surrounded by rhombuses with equivalent edges. This modified polyhedron is called a rhombus dodecahedron [8]. The polyhedron in Fig. 2.40e is produced by cutting corners of a cube (Fig. 2.40f) or an octahedron (Fig. 2.40g), and called a truncated cube or truncated octahedron. This polyhedron is surrounded by squares and hexagons with equivalent edges. Note that we can fill the whole three-dimensional space by stacking these polyhedra attaching a hexagon face to a hexagon and a square face to a square. Not only this polyhedron but also all Brillouin zones fulfill this condition. The Brillouin zone of a triclinic system has a complicated shape (Fig. 2.40a), but can fill the whole three-dimensional space. This is obvious because these polyhedra are surrounded by perpendicular bisectors of lattice points. The body-center and face-center cubic lattices involve more than two lattice points, but the Brillouin zone contains only a single Γ point. In general, the Brillouin zone is a minimal repeating unit centered at the Γ point.

Example 2.10 Identify the point groups of Fig. 2.40d, e.

Both are O_h .

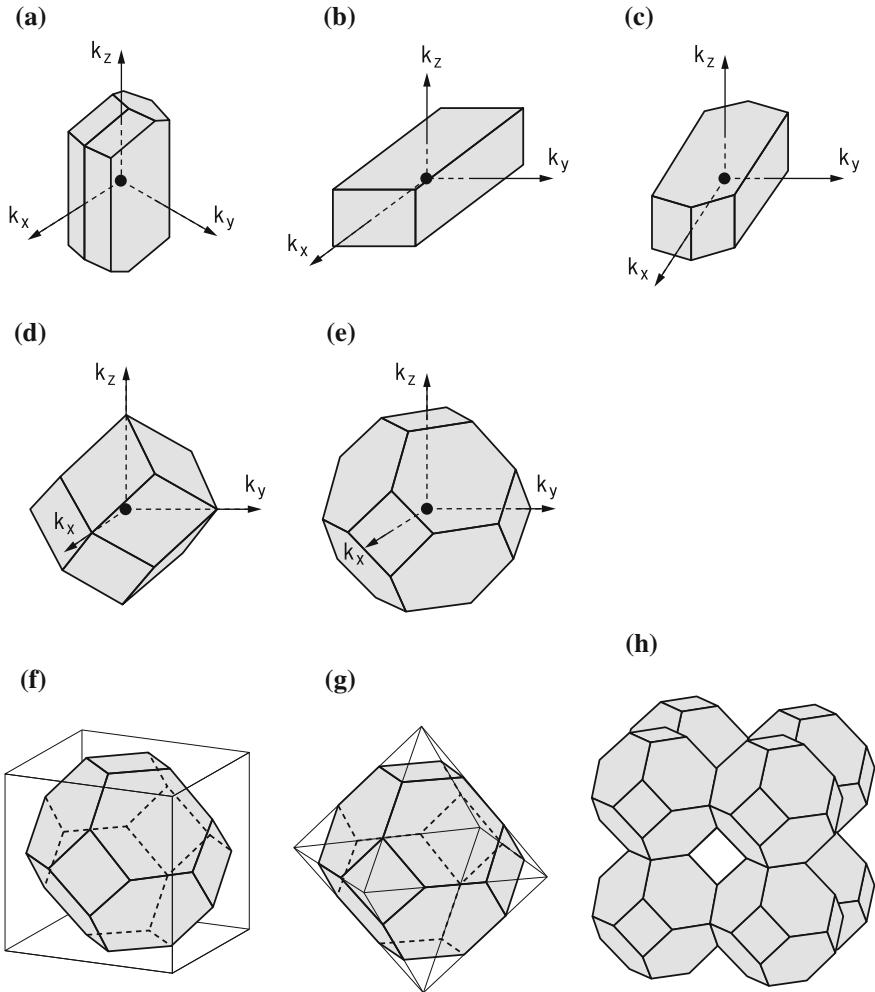
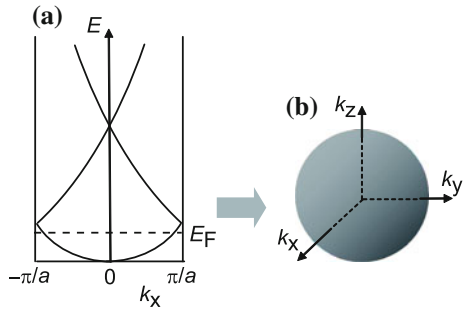


Fig. 2.40 Three-dimensional Brillouin zones. **a** Triclinic. **b** Orthorhombic P. **c** Orthorhombic C. **d** Body-center cubic. **e** Face-center cubic. **f** Truncated cubic. **g** Truncated octahedron. **h** Face-center cubic

2.8 Fermi Surface of Metals

Next, we discuss the Fermi surface of metals [9]. Alkali metals such as sodium and potassium have a body-center lattice, and the Brillouin zone is represented by Fig. 2.40d. When one electron enters the energy band, the volume of the Fermi surface is half the first Brillouin zone, because the s band receives up to two electrons. So the Fermi surface is a sphere and does not touch the zone boundary

Fig. 2.41 Spherical Fermi surface of an alkali metal



(Fig. 2.41). Experimental methods described in Sect. 3.4 have proved the deviation from the perfect sphere is less than 1 %.

Alkali earth metals such as magnesium and calcium have two valence electrons, and the volume of the Fermi surface is equal to the Brillouin zone. Accordingly, the Fermi surface spread out of the first Brillouin zone (Fig. 2.42). These metals have a hexagonal or body-center lattice, but a square lattice is schematically depicted in Fig. 2.42. In the first Brillouin zone, the shaded region is occupied as shown in Fig. 2.42c. Holes exist in the white region to make a star-like hole pocket at the corner. In the second Brillouin zone, the shaded region in Fig. 2.42d is occupied to make an elliptical electron pocket. Like this, starting from a naive free-electron model, we can predict fairly complicated electron and hole pockets. Such a Fermi surface has been proved by actual experiments. The group 3 and 4 elements have a similar Fermi surface.

The Fermi surface of a transition metal is similarly composed of many electron and hole pockets. However, we shall investigate the global feature (Fig. 2.43a). For example, electron configuration of a titanium atom is $4s^23d^2$. In the solid metal, the s band is larger than the d band, and the s band spreads over the d band. Then, it is appropriate to approximate that the s band has one electron, and other electrons enter the d band like $4s^13d^3$. In elemental metals, the electron configuration is generally represented by s^1d^{n-1} . Since the five d orbitals can receive up to ten electrons, six-electron systems such as chromium, molybdenum, and tungsten have

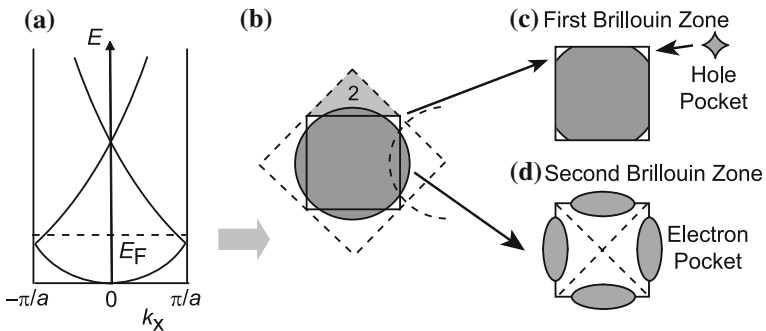


Fig. 2.42 Fermi surface of an alkali earth metal

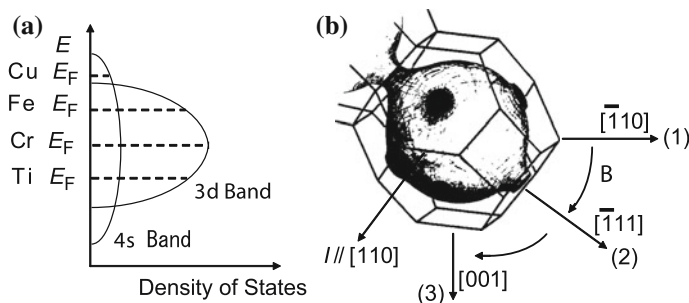


Fig. 2.43 a Energy bands of transition metals. b Fermi surface of copper

s^1d^5 configuration, and the Fermi energy is located at the center of the d band. The d band is composed of many energy bands, but the density of states is maximum at the band center. Since the metal electrons constitute a kind of covalent bonds, these metals form strong chemical bonds with the surrounding atoms. This is the reason that these metals exhibit the highest melting points among all elements.

Iron metal has $4s^13d^7$ configuration, and the d band is mostly occupied up to the upper end. Copper metal has $4s^13d^{10}$ configuration, and the d band is entirely occupied. Since the s band has one electron, the Fermi surface is almost spherical similarly to alkali metals (Fig. 2.43b), where the volume of the Fermi sphere is half the Brillouin zone. Copper has a face-center cubic lattice, and the Brillouin zone is represented by Fig. 2.40e. However, the Fermi surface of copper touches the zone boundary, and is connected to the adjacent Fermi sphere (Fig. 2.43b). The presence of such a connected Fermi surface has been proved experimentally (Sect. 3.5).

2.9 Fermi Surface of Low-Dimensional Metals

There are examples of one- and two-dimensional metals. A platinum complex with the composition of $K_2[Pt(CN)_4]Br_{0.3x}H_2O$ forms a one-dimensional conductor called KCP (Fig. 2.44a). Platinum forms a square-planar complex like $[Pt(CN)_4]^{2-}$, which is stacked to form a one-dimensional Pt–Pt chain ($//c$). When partially oxidized with bromine, the one-dimensional band composed of the Pt d_{z^2} orbitals is partially filled. This complex shows metallic conductivity around room temperature, but undergoes a Peierls transition at 250 K, below which the platinum chain is distorted according to the $2k_F = 0.30 c^*$ periodicity.

One-dimensional columns of $NbSe_3$ are composed of trigonal prisms (Fig. 2.44b). Since a unit cell contains three different columns, there are three different sheets of the Fermi surface. Therefore, $NbSe_3$ undergoes the Peierls transitions twice at 143 and 53 K. However, the interchain interaction is too large to make the columns entirely insulating. Then, after the resistance once goes up, a metallic decrease is restored again.

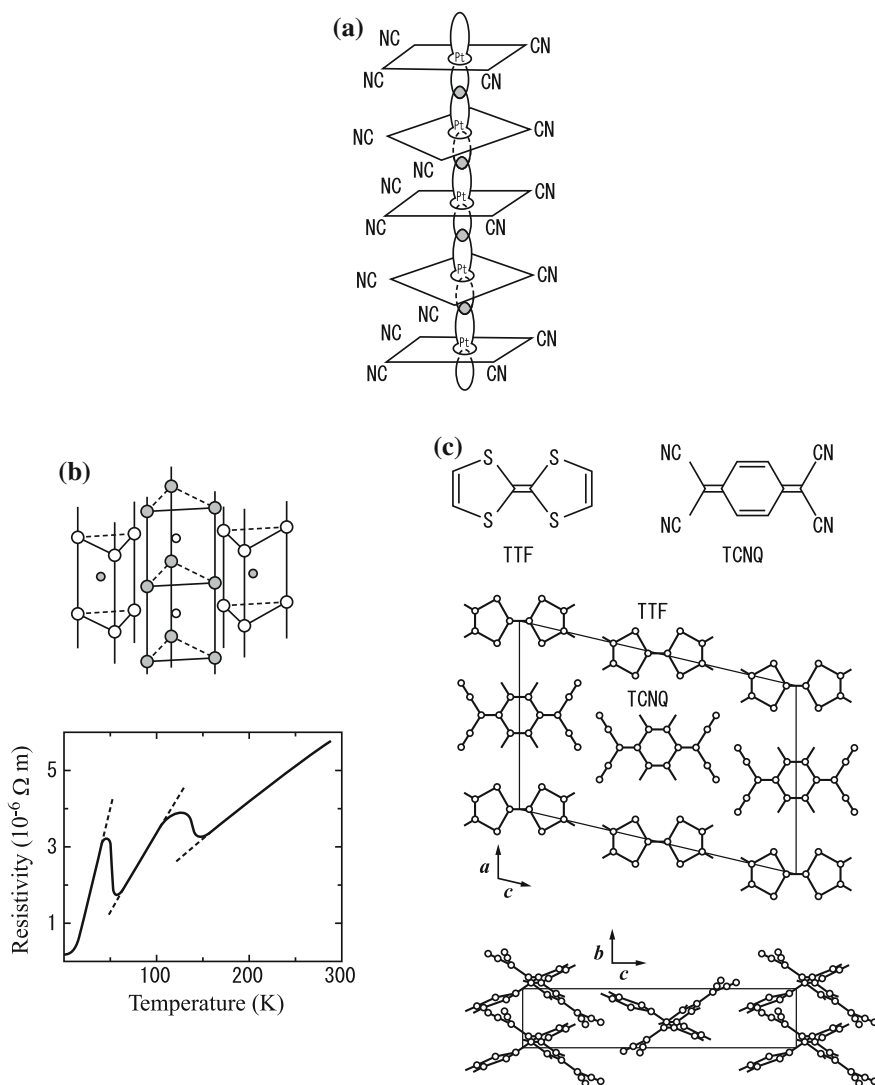


Fig. 2.44 One-dimensional metals: (a) KCP, (b) structure and resistivity of NbSe₃, and (c) (TTF) (TCNQ)

Many organic conductors consist of planar molecules with an extended π -electron system, and tend to form one-dimensional conductors (Sect. 7.4). Figure 2.44c shows a typical one-dimensional organic charge-transfer complex composed of tetrathiafulvalene (TTF) and tetracyanoquinodimethane (TCNQ). The conductivity is highest along the stacking (*b*) axis.

Organic conductors are usually one-dimensional. Therefore, ordinary organic conductors undergo a Peierls transition and become insulating at low temperatures.

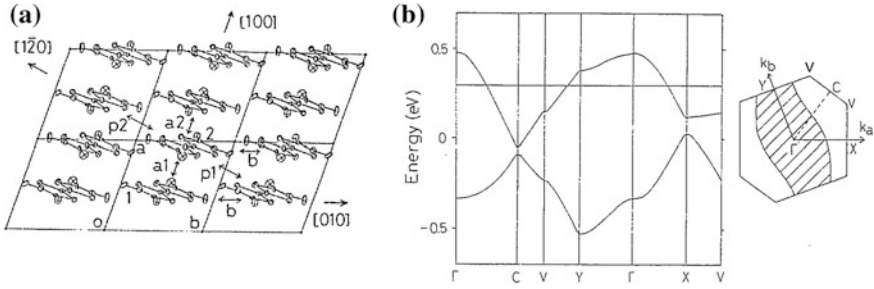


Fig. 2.45 (a) Crystal structure and (b) energy band of $(\text{TMTSF})_2\text{PF}_6$. The transfer integrals are $\beta_{a1} = 200$, $\beta_{a2} = 230$, $\beta_b = 35$, $\beta_{p1} = 20$, and $\beta_{a1} = 7$ meV

In order to make organic superconductors, it is necessary to suppress the Peierls transition and to maintain the metallic conductivity down to low temperatures. For this purpose, two-dimensional organic conductors have been explored. Figure 2.45 shows the crystal structure of the first organic superconductor, $(\text{TMTSF})_2\text{PF}_6$ (TMTSF: tetramethyltetraselenafulvalene in Fig. 7.16). TMTSF has many molecular orbitals, but to investigate the electronic properties, it is sufficient to consider the molecular orbital in which the Fermi energy is located. From the composition, TMTSF has $1/2+$ charge, so we only consider the partially filled HOMO. A unit cell contains two molecules designated as 1 and 2 (Fig. 2.45a), and the secular equation is derived similar to Eqs. 2.80 and 2.82.

$$\begin{vmatrix} \beta_{11} - E & \beta_{12} \\ \beta_{21} & \beta_{22} - E \end{vmatrix} = 0$$

$$\beta_{11} = \beta_{22} = \beta_b e^{ik_b b} + \beta_b e^{-ik_b b} = 2\beta_b \cos k_b b$$

$$\beta_{12} = \beta_{21}^* = \beta_{a1} + \beta_{a2} e^{-ik_a a} + \beta_{p1} e^{-ik_b b} + \beta_{p2} e^{-i(k_a a - k_b b)} \quad (2.88)$$

Here, α is omitted. Molecule 1 is sandwiched by two Molecules 1 located at $\pm b$, to which the central molecule is connected by β_b . This forms β_{11} . Molecule 2 is similarly related to Molecules 2 in the adjacent $\pm b$ cells, and β_{22} has the same form. The interaction between Molecule 1 and Molecule 2 (β_{12}) consists of β_{a1} and β_{a2} in the $\pm a$ directions, in addition to β_{p1} and β_{p2} in the oblique direction. The secular equation is reduced to

$$(\beta_{11} - E)^2 = \beta_{12} \beta_{12}^*. \quad (2.89)$$

The insertion of β_{ij} affords the solutions. However, it is more convenient to multiply $e^{ik_a a/2}$ to β_{12} .

$$\beta_{12}e^{ik_a a/2} = \beta_{a1}e^{ik_a a/2} + \beta_{a2}e^{-ik_a a/2} + \beta_{p1}e^{i(k_a a/2 - k_b b)} + \beta_{p2}e^{-i(k_a a/2 - k_b b)} \quad (2.90)$$

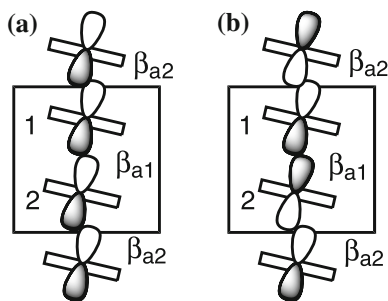
and $e^{-ik_a a/2}$ is multiplied to β_{12}^* . It is generally possible to multiply this kind of an arbitrary phase. Equation 2.88 is written assuming both Molecules 1 and 2 are located in the same cell, but Eq. 2.90 is obtained supposing Molecule 2 is placed at $a/2$. The energy band is represented by using $\Delta = \beta_{12} \beta_{12}^*$.

$$E(k) = 2\beta_b \cos(k_b b) \pm \sqrt{\Delta}$$

$$\Delta = \left[(\beta_{a1} + \beta_{a2}) \cos\left(\frac{k_a a}{2}\right) + (\beta_{p1} + \beta_{p2}) \cos\left(\frac{k_a a}{2} - k_b b\right) \right]^2 + \left[(\beta_{a1} - \beta_{a2}) \sin\left(\frac{k_a a}{2}\right) + (\beta_{p1} - \beta_{p2}) \sin\left(\frac{k_a a}{2} - k_b b\right) \right]^2. \quad (2.91)$$

The transfer integrals are estimated from the molecular orbital calculation as listed in the caption of Fig. 2.45. Through use of these values, the energy band is calculated as shown in Fig. 2.45b. The Brillouin zone is represented by a hexagon because the unit cell is triclinic (Figs. 2.39 and 2.40a). The energy bands are plotted starting from the Γ point to the upper right C point, followed by the anticlockwise rotation to V, Y, Γ , and X, to go to another V point. Since a unit cell contains two molecules, Eq. 2.89 is a quadratic equation and affords two energy bands. The 1/2+ charge of the TMTSF molecule implies the HOMO band is 3/4-filled, and the upper 1/4 is empty. The hole part corresponds to the shaded region in the Brillouin zone. The shaded parts are chosen from the top of the energy band until the shaded area becomes half the Brillouin zone. The boarder of the shaded region is a winding curve extending in the b^* direction, so the warping Fermi surface extending in the b^*c^* direction indicates a one-dimensional metal along the a axis. This is associated with β_{a1} and β_{a2} , which are ten times larger than the other transfers. The interchain transfers, however, make the Fermi surface considerably warping. As a

Fig. 2.46 π orbitals of $(\text{TMTSF})_2\text{PF}_6$



result, this complex maintains the metallic conductivity down to 12 K and exhibits superconductivity at 0.9 K under pressure.

All transfer values are positive (Fig. 2.45 caption), but this is accidental. If the π orbitals are defined as Fig. 2.46a, the overlap integrals are negative, and the transfer integrals are positive. However, if the sign of the molecular orbital on Molecule 2 is taken opposite (Fig. 2.46b), the overlap integrals are positive, and the transfer integrals are negative. It is always possible to choose the signs of the basis functions arbitrarily. Since the transfer β_b connects the same kind of molecules, the sign is uniquely defined. In Eq. 2.91, all transfers except for β_b appear as the squares, so even if all these transfers are taken negative, the resulting energy band is unchanged. Like this, the signs of the transfer integrals are changeable as far as the signs are chosen systematically according to the basis functions.

Example 2.11 Figure 2.47 is a popular structure of organic crystals, known as the θ -phase or a herringbone structure. Obtain the equation of the energy band.

For simplicity, we assume $\alpha = 0$. A unit cell contains two shaded molecules, where β_a connects the same molecules (1-1 or 2-2) in the $\pm a$ direction, and β_p connects the different molecules (1-2) in the diagonal directions ($\pm a/2, \pm b/2$). Obtain the element β_{11} and β_{12} , and calculate the formula of the energy band $E(k_a, k_b)$.

1. Viewed from the shaded Molecule 1, Molecules 1 in the adjacent $+a$ and $-a$ cells are connected by the transfer integral β_a . Then, we obtain the diagonal element.

$$\beta_{11} = \beta_a e^{ik_a a} + \beta_a e^{-ik_a a} = 2\beta_a \cos k_a a \quad (2.92)$$

Note that β_{22} has the same form.

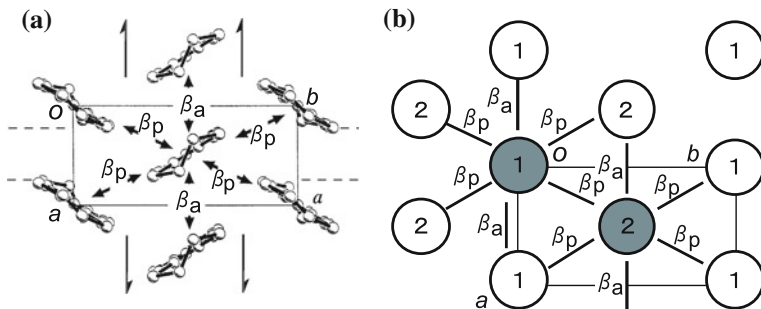


Fig. 2.47 Structure of the θ -phase. The transfer integrals are $\beta_a = 25$ and $\beta_p = 101$ meV

2. Viewed from the central shaded Molecule 1, four Molecules 2 in the $(\pm a/2, \pm b/2)$ directions are connected by the transfer integral β_p . Then, we obtain the non diagonal element.

$$\begin{aligned}\beta_{12} &= \beta_p e^{i\frac{k_a a + k_b b}{2}} + \beta_p e^{-i\frac{k_a a + k_b b}{2}} + \beta_p e^{i\frac{k_a a - k_b b}{2}} + \beta_p e^{-i\frac{k_a a - k_b b}{2}} \\ &= 2\beta_p \left(\cos \frac{k_a a + k_b b}{2} + \cos \frac{k_a a - k_b b}{2} \right)\end{aligned}\quad (2.93)$$

3. $\begin{vmatrix} \beta_{11} - E & \beta_{12} \\ \beta_{12} & \beta_{11} - E \end{vmatrix} = 0$ leads to $E = \beta_{11} \pm \beta_{12}$. The results of (1) and (2) are substituted in this formula.

$$\begin{aligned}E &= 2\beta_a \cos k_a a \pm 2\beta_p \left(\cos \frac{k_a a + k_b b}{2} + \cos \frac{k_a a - k_b b}{2} \right) \\ &= 2\beta_a \cos k_a a \pm 4\beta_p \cos \frac{k_a a}{2} \cos \frac{k_b b}{2}\end{aligned}\quad (2.94)$$

When the transfer integrals obtained from the molecular orbital calculation (Fig. 2.47 caption) are placed in this equation, the energy band is obtained as shown in Fig. 2.48. The two-dimensional network affords the elliptical Fermi surface.

Since a unit cell contains two molecules, there are two energy bands in Fig. 2.48. However, on the CX and CY zone boundaries, the energy bands are degenerate to one. This is due to the two-fold screw axis along the a axis and the glide plane along the b axis (Fig. 2.47a). A molecule has symmetry elements such as rotation, inversion, and mirror, but a space group in a crystal has additional symmetry elements such as a screw axis and a glide plane, in which translation is combined

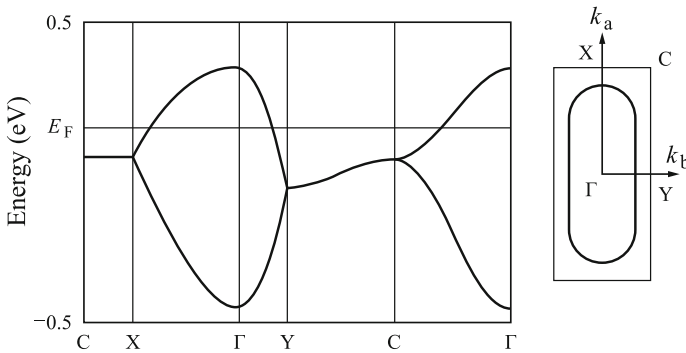


Fig. 2.48 Energy band in the θ -phase

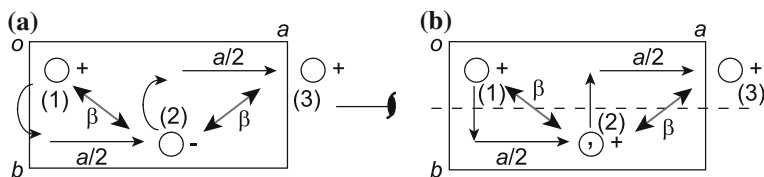


Fig. 2.49 (a) A screw axis, and (b) a glide plane

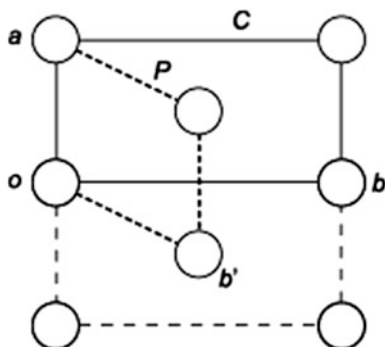
with rotation and mirror, respectively. A **two-fold screw axis** is a combination of two-fold rotation and translation, where after the 180° rotation, the atom is translated by $a/2$ (Fig. 2.49a). The symbols + and - represent an atom located above and below the sheet. Then, the atom (1) moves to (2). One more operation moves (2) to (3), which corresponds to a one-unit-cell (a) translation of (1). In a **glide plane** (b), the original atom (1) is reflected, and translated by $a/2$ to (2). The comma implies, if the original atom has right-hand chirality, the atom with comma has left-hand chirality. One more operation moves (2) to (3), which is again the a translation.

The transfer integral between (1) and (2) is equivalent to the transfer integral between (2) and (3), because they are generated by the same symmetry operation applied to the crystallographically equivalent molecules. Accordingly, although the periodicity of the crystal is a , the periodicity of β is $a/2$. This is the origin of the degenerate zone boundary in Fig. 2.48. This is just opposite to the Peierls transition (Fig. 2.35a), where at $\beta_1 = \beta_2$, the energy band is similarly degenerated at $2\pi/a$. Space groups including symmetry operations with translation such as a screw axis and a glide plane are called **non-symmorphic** [10]. In general, energy bands of non-symmorphic space groups are degenerate at the zone boundary in the direction of the translation. The band structure of the θ -phase (Fig. 2.48) is degenerate both along the a and b axes, respectively, owing to the screw axis and the glide plane. This is obvious because two β_p are repeated in the unit cell both along the a and b axes.

In a molecule, the secular equation is reduced to separate blocks according to the symmetry, and energy levels belonging to different symmetry are independently obtained. In a crystal, such block diagonalization does not work because the symmetry disappears at the general k point even when the crystal has symmetry. Then, the degeneracy at the zone boundary in a non-symmorphic space group is an important conclusion derived from the symmetry. Even in a triclinic lattice, special points such as Γ , X, Y, and C have inversion symmetry. At these points, all elements in the secular equation become real, and the energy levels are classified to symmetrical (gerade) and antisymmetrical (ungerade). These special points are important to discuss the electronic structure of graphene.

C-center cells have two lattice points in a unit cell. For the band calculation, the C-center cell is transformed to a primitive cell (Fig. 2.50). The resulting cell has oblique axes, where a monoclinic cell is transformed to a triclinic cell, and orthorhombic turns to monoclinic. The resulting cell contains a single lattice point, and the volume is half of the original cell. The volume of the Brillouin zone

Fig. 2.50 Transformation from a C-center lattice to a primitive lattice



corresponding to the primitive cell is twice of the volume assuming the C-center cell. Then, the energy bands are represented in the extended zone scheme. When we use the Brillouin zone of the C-center cell, the energy bands are folded into the reduce zone, and the number of the energy bands are twice larger, corresponding to the original two lattice points.

The transfer integrals are calculated on the basis of molecular orbitals of the single molecule. For an electron donor, we calculate the transfer integrals between the HOMO. According to the spirit of the extended Hückel approximation, the transfer integrals are obtained from Eq. 1.28.

$$\beta_{kl} \approx \int \psi_k H \psi_l d\tau = E S_{kl}$$

Then, the transfer integrals β_{kl} are estimated from the overlap integrals S_{kl} by multiplying the HOMO energy E . In general, $E = -10$ eV is used because this value affords good agreement with the experiments. Since the HOMO is represented by LCAO (Eq. 1.23) of the atomic orbitals χ_i , the overlap integral S_{kl} is

$$S_{kl} = \sum_i \sum_j c_i c_j \int \chi_i \chi_j d\tau.$$

First, we evaluate the overlap integrals between χ_i and χ_j . Then, c_i and c_j are multiplied, and S_{kl} is obtained. The values of c_i and c_j are taken from the molecular orbital calculation. The transfer integrals listed in the captions of Figs. 2.45 and 2.48 are obtained like this.

The overlap integral S_{kl} between two BEDT-TTF molecules is plotted in Fig. 2.51 as a function of the angle φ between the molecular plane and the intermolecular vector. Along the stack ($\varphi = 90^\circ$), S_{kl} is about -20×10^{-3} . By multiplying $E = -10$ eV, the corresponding transfer integral is 0.2 eV. Then, the one-dimensional stack gives the bandwidth of $4\beta = 0.8$ eV. The overlap integral has additional peaks at 60° , 30° , and 0° . The sign of the overlap integral is unimportant when the energy band is formed. Between these peaks, the overlap

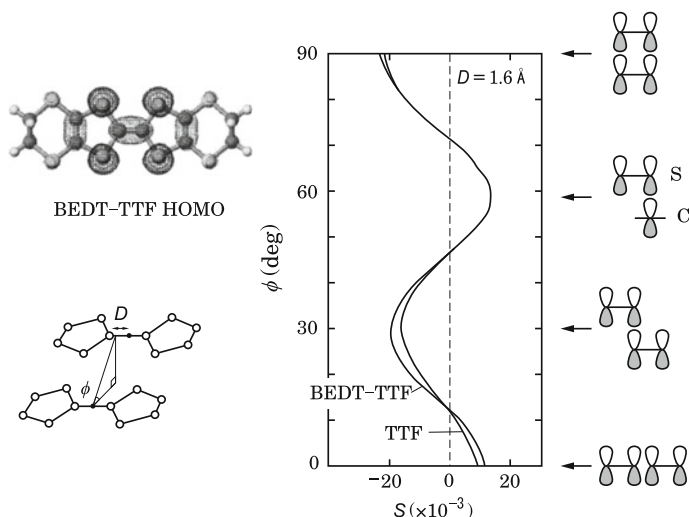


Fig. 2.51 Orientation dependence of the overlap integral between the HOMO of two BEDT-TTF molecules [11]

integral crosses zero. It is not certain whether the β zero coming from the HOMO phase is related to some physical properties. However, the angle dependence of the overlap integral is sometimes very important in determining the systematic change of the properties of organic conductors (Sect. 7.7.4). Instead of the direct calculation of the overlap integrals, molecular orbital calculation is sometimes carried out for two molecules. The HOMO splitting corresponds to the bonding and antibonding combinations, and gives 2β . Since the molecular orbitals change depending on the dimer geometry, this method does not afford $\beta = 0$.

Bandwidths of the representative organic conductors are listed in Table 2.1 [12–18]. It is obvious from Eq. 2.92 that the bandwidth of the θ -phase is $4|\beta_a| + 8|\beta_p|$.

Table 2.1 Bandwidths of the representative organic conductors

Compound	Bandwidth/eV	References
(TMTSF) ₂ X	1.0	
(BEDT-TTF) ₂ X	1.0	
Pentacene HOMO	0.2	[12, 13]
Rubrene HOMO	0.34	[14]
Picene HOMO	0.27	[13]
Sexithiophene HOMO	0.2	[13]
M(TCNQ)	1.0	
C ₆₀ LUMO	0.5	[15, 16]
La _{2-x} Sr _x CuO ₄	2	[17]
Graphene	10	[18]

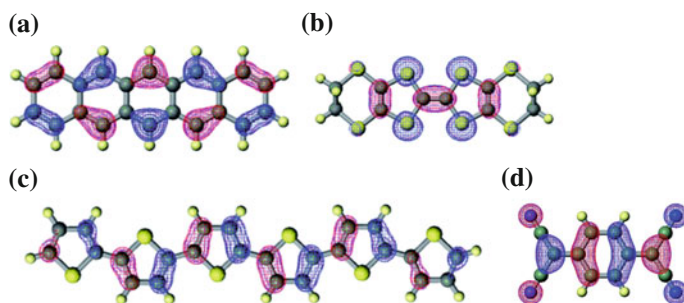


Fig. 2.52 Molecular orbitals of the representative organic conducting molecules. The *shaded regions* depend on the molecular orbital signs. **a** Pentacene HOMO. **b** BEDT-TTF HOMO. **c** Sexithiophene HOMO. **d** TCNQ LUMO

Note that in organic charge-transfer complexes like $(\text{BEDT-TTF})_2\text{X}$, the energy band is quarter-filled, but in organic semiconductors like pentacene and thiophene, the HOMO is entirely occupied. Bandwidths of TTF family charge-transfer complexes are usually about 1.0 eV.

The bandwidths are determined by the overlap of the atomic orbitals. The exponent is $\zeta = 1.625$ for C 2p, whereas $\zeta = 1.817$ for S 3p (Appendix 2). As shown in Fig. 1.5, the smaller is ζ , the larger is the orbital. For the same ζ , however, 3p is larger than 2p. The van der Waals distance is 1.70 Å for C, while 1.85 Å for S [19]. Therefore, the atomic orbital of S affords much larger overlap than C. 1 eV bandwidth of the TTF family mainly comes from this S-S overlap.

Molecular orbitals of the representative organic conductors are shown in Fig. 2.52. Four sulfur atoms in TTF have the same sign; this is advantageous to give a large overlap without largely depending on the orientation [11, 13]. In pentacene, the HOMO is mostly located on the carbon atoms, and the side hydrogen atoms prohibit the transverse interaction. However, the herringbone structure realizes the two-dimensional band. The HOMO of thiophene has nodes on the sulfur atoms, and the coefficients are zero. Then, the S-S overlap does not contribute to the bandwidth. The calculated bandwidth of oligothiophene is as small as that of pentacene (0.2 eV). However, the next HOMO has a finite coefficient on sulfur, and this contribution enlarges the bandwidth as large as 0.4 eV. TCNQ does not contain sulfur atoms, but forms an energy band as large as 1 eV along the stack. The LUMO bandwidth of C_{60} is around 0.4 ~ 0.5 eV, and the density of states is enhanced due to the three-fold degeneracy. Bandwidth of inorganic compounds with connected chemical bonds is large; for example, 2 eV for the $d_{x^2-y^2}$ band in the CuO plane of the copper oxide superconductors (Fig. 2.31) [11]. The bandwidth of graphite and graphene comes from the C = C covalent bonds, which is as large as 10 eV.

References

1. R. Hoffmann, *Solids and Surfaces: A Chemist's View of Bonding in Extended Structures* (Wiley, Hoboken, 1988)
2. J.-M. André, J. Delhalle, J.-L. Brédas, *Quantum Chemistry Aided Design of Organic Polymers* (World Scientific, 1991)
3. C. Kittel, *Introduction to Solid State Physics*, 8th edn. (Wiley, Hoboken, 2004)
4. N.W. Ashcroft, N.D. Mermin, *Solid State Physics* (Thomson, 1976)
5. H. Ibach, H. Luth, *Solid State Physics* (Springer, Berlin, 1993)
6. N.F. Mott, H. Jones, *The Theory of Properties of Metals and Alloys* (Dover, 1958)
7. R.E. Peierls, *Quantum Theory of Solids* (Clarendon, 1956)
8. P.R. Cromwell, *Polyhedra* (Springer, Berlin, 1997)
9. A.P. Cracknell, K.C. Wong, *The Fermi Surface* (Clarendon, 1973)
10. G. Burns, *Introduction to Group Theory with Applications* (Academic Press, Cambridge, 1977)
11. T. Mori, A. Kobayashi, Y. Sasaki, H. Kobayashi, G. Saito, H. Inokuchi, *Bull. Chem. Soc. Jpn.* **57**, 627 (1984)
12. R.C. Haddon, T. Siegrist, R.M. Fleming, P.M. Bridenbaugh, R.A. Laudise, *J. Mater. Chem.* **5**, 1719 (1995)
13. H. Kojima, T. Mori, *Bull. Chem. Soc. Jpn.* **84**, 1049 (2011)
14. D.A. de Silva Filho, E.G. Kim, J.L. Bredas, *Adv. Mater.* **17**, 1072 (2005)
15. R.C. Haddon, X. Chi, M.E. Itkis, J.E. Anthony, D.L. Eaton, T. Siegrist, C.C. Mattheus, T.T.M. Pastra, *J. Phys. Chem.* **16**, 433 (2002)
16. M.S. Dresselhaus, G. Dresselhaus, P.C. Eklund, *Science of Fullerenes and Carbon Nanotubes* (Academic Press, Cambridge, 1996)
17. C.P. Poole, H.A. Farach, R.J. Creswick, *Superconductivity* (Academic Press, Cambridge, 1995)
18. A. Zunger, *Phys. Rev. B* **17**, 626 (1978)
19. F.A. Cotton, G. Wilkinson, *Inorganic Chemistry* (Interscience, 1962)



<http://www.springer.com/978-4-431-55263-5>

Electronic Properties of Organic Conductors

Mori, T.

2016, X, 356 p. 288 illus., 34 illus. in color., Hardcover

ISBN: 978-4-431-55263-5